INVESTIGATION OF CONSTRAINTS
IN THERMAL SIMILITUDE

VOLUME II

P. L. MILLER

F. W. HOLM

173,816

Distribution of this document is unlimited.

FOREWORD

This report has been prepared by the Mechanical Engineering Department, Kansas State University, Manhattan Kansas as part of U. S. Air Force Contract F 33615-68-C-1017, "Investigation of Constraints in Thermal Similitude". The work was administered under the direction of Air Force Flight Dynamics Laboratory, Air Force Systems Command, with Mr. Carl J. Feldmanis FDFE Project Engineer. The work was performed between September 1967 and September 1969 with Dr. P. L. Miller as Principal Investigator.

Manuscript released by the authors 1 September 1969.

This technical report has been reviewed and is approved

William C. Savage, Chief
Environmental Control Branch
Vehicle Equipment Division
A F Flight Dynamics Laboratory

ABSTRACT

The studies described in this report clarify the effects of some of the limitations imposed by the laws of thermal similitude, and determine the thermal modeling laws for a heat pipe.

Solutions were presented for the steady-state temperature distribution and heat transfer in a radiating fin having temperature dependent thermal conductivity. Using these solutions, modeling prediction errors were determined for fin type prototype/model systems with dimensional distortions, with material having temperature dependent thermal conductivity, and with low prototype temperatures. These prediction discrepancies ranged from very small errors to errors in heat transfer rate as high as 75% in a severely distorted model.

The thermal modeling laws for a heat pipe were derived and experimentally verified. It was observed that prototype thermal behavior could be predicted, from model data, to within 10°F over the temperature range tested (140 to 330°F). Heat pipe failure due to capillary failure was also predictible to within ±10%.

A flexible heat pipe was also designed and experimentally tested. Performance was not degraded under conditions of bending.

iv

TABLE OF CONTENTS

LIST OF FIGURES

vi

LIST OF TABLES

LIST OF SYMBOLS

A_1 mean area of wick normal to the radial direction, sqft

A_2 mean area of the wall normal to the radial direction, sqft

A_c outer surface area of the condenser, sqft

A_e cross-sectional area of pores in wick normal to liquid flow, sqft

A_E surface area of the evaporator liquid-wick-vapor interface, sqft

A_T total cross-sectional area of the wick normal to liquid flow, sqft

C_1 constant

C_2 constant

g acceleration of gravity, ft/sec^2

g_c gravitational constant $lb_m ft/lb_f sec^2$

h_{fg} latent heat of vaporization, btu/lb

h_f enthalpy of the liquid, btu/lb

h_g enthalpy of the vapor, btu/lb

k specific permeability of the wick

K_1 thermal conductivity of the wick, btu/(hr sqft F)

K_2 thermal conductivity of the wall, btu/(hr sqft F)

L length, ft

L_a length of adiabatic section, ft

L_c length of condenser section, ft

L_e length of evaporator section, ft

L_T total length of heat pipe, ft

$\dot{m}_g$ vapor flow rate, lb/sec

$\dot{m}_f$ liquid flow rate, lb/sec

$\dot{m}_T$ total mass percolating through the heat pipe per unit time, lb/sec

N water parameter, $\dfrac{h_{fg}\rho_f\sigma_f}{\mu_f}$

P pressure, lb/sqft

q rate of heat transfer, btu/hr

r radial direction, ft

r_1 inside wick radius, ft

r_2 outside wick radius, ft

r_3 outside wall radius, ft

R radius of curvature of the liquid-vapor interface, microns

R_v gas constant for water vapor

T_v temperature of the vapor, °R

T_o temperature of the condenser outer wall, °R

u velocity in the x-direction, ft/sec

v velocity in the r-direction, ft/sec

v_i vapor injection velocity, ft/sec

v_s vapor suction velocity, ft/sec

x axial direction, ft

Z thermal resistance to heat conduction, (ft hr °F)/btu

α mass transfer accommodation coefficient

ϵ emittance

θ angle inclination of the heat pipe with respect to g, radians

μ absolute viscosity, $(lb_f sec)/sqft$

x

LIST OF SYMBOLS (cont.)

π 3.14159...

ρ density , lb/cuft

σ surface tension , lb/ft

σ_o Stefan-Boltzmann constant , btu/(hr sqft $°R^4$)

SECTION I

INTRODUCTION

To accurately predict the thermal behavior of a space craft, it is desirable to test a full scale prototype inside an environmental simulator. Proper environmental simulation requires conditions of high vacuum, cold wall radiant energy sinks, and solar, planet, and albedo radiation. Existing and potential space craft exceed the capabilities of earth-bound environmental simulators because of their large size, and this creates a problem for the experimenter.

One solution to this problem has been thermal scale modeling. A thermal scale model can be defined as a model different in size (generally smaller) than its prototype, which under suitable conditions will accurately predict the thermal behavior of its prototype (1). For conduction-radiation coupled systems it has been shown that the laws governing thermal scale modeling will accurately predict thermal behavior between model and prototype (2). Systems coupled by additional modes of heat transfer require additional consideration.

The heat pipe couples all three modes of heat transfer; that is, conduction, convection, and radiation. The usefulness of a heat pipe stems from its ability to exhibit an extremely high effective thermal conductivity, much greater in fact than any known homogeneous material. The comparison of a heat pipe to a homogeneous material is unfair however, since a heat pipe

1

is not homogeneous throughout. A heat pipe consists of a closed cylindrical container with a porous wick lining. Liquid saturates the wick of a heat pipe and vapor occupies the remaining volume. When heat is added to (or rejected from) the container, liquid vaporizes where heat is added and vapor condenses where heat is extracted, maintaining nearly constant temperature throughout. The condensate is returned to the evaporator by the action of capillary forces in the wick.

The defining equations for heat pipe operation form a system of simultaneous differential equations, for which no solution has been obtained. As suggested by Cosgrove (3), a study of the thermal behavior of a heat pipe is of utmost importance since there is no procedure available for predicting the heat pipe temperature at a given heat flux.

Because there is no solution available for these differential equations, and because heat pipe configurations will become larger and more complex in future applications, a thermal scale modeling program was instituted for the purpose of providing a method for predicting the performance characteristics of a heat pipe from the experimental behavior of a dimensionally and thermally similar (model) heat pipe.

The equations derived in this study are for two specific modeling techniques: 1. a technique preserving materials between model and prototype, and 2. a technique maintaining the same heat flux in both model and prototype. The similarity relations for the first modeling technique were verified by

experiment and the similarity relations for the second modeling

technique are presented without experimental verification. The

model and prototype were tested in a high vacuum, cold wall

environment without simulated solar, planet, or albedo radia-

tion.

Incidental to this study, a separate investigation has sought to demon-

strate the feasibility of constructing and operating a flexible heat pipe.

This work was undertaken preliminary to the heat pipe modeling program and

served to provide initial guidance and experience in the technology of heat

pipes.

SECTION II

THERMAL SCALE MODELING OF A HEAT PIPE

1. SIMILARITY ANALYSIS

One procedure for obtaining the dimensionless groups used in thermal scale modeling requires knowledge of the form of the differential equations describing the thermal behavior of the prototype. Since the differential equations for heat transfer are well known, the thermal behavior of the prototype can usually be described by a set of simultaneous differential equations. A similar set of differential equations must apply to both model and prototype. By non-dimensionalizing the sets of differential equations, they become identical and the dimensionless groups in these equations form the basis for thermal scale modeling even though the differential equations are not amenable to solution.

Figure 1 illustrates the various mechanisms of heat and mass transfer that occur in an active heat pipe. Heat is transferred radially inward from the source by thermal conduction through the wall and wick of the heat pipe. Liquid is vaporized in the wick and travels along the axis of the heat pipe as condensation occurs on the inside surface of the wick in the condenser. Heat is then transferred by conduction through the wick and wall of the condenser and is finally rejected at the surface of the condenser by radiation.

The heart of heat pipe operation is the wick, which provides the capillary pumping action for returning the condensate to the evaporator.

4
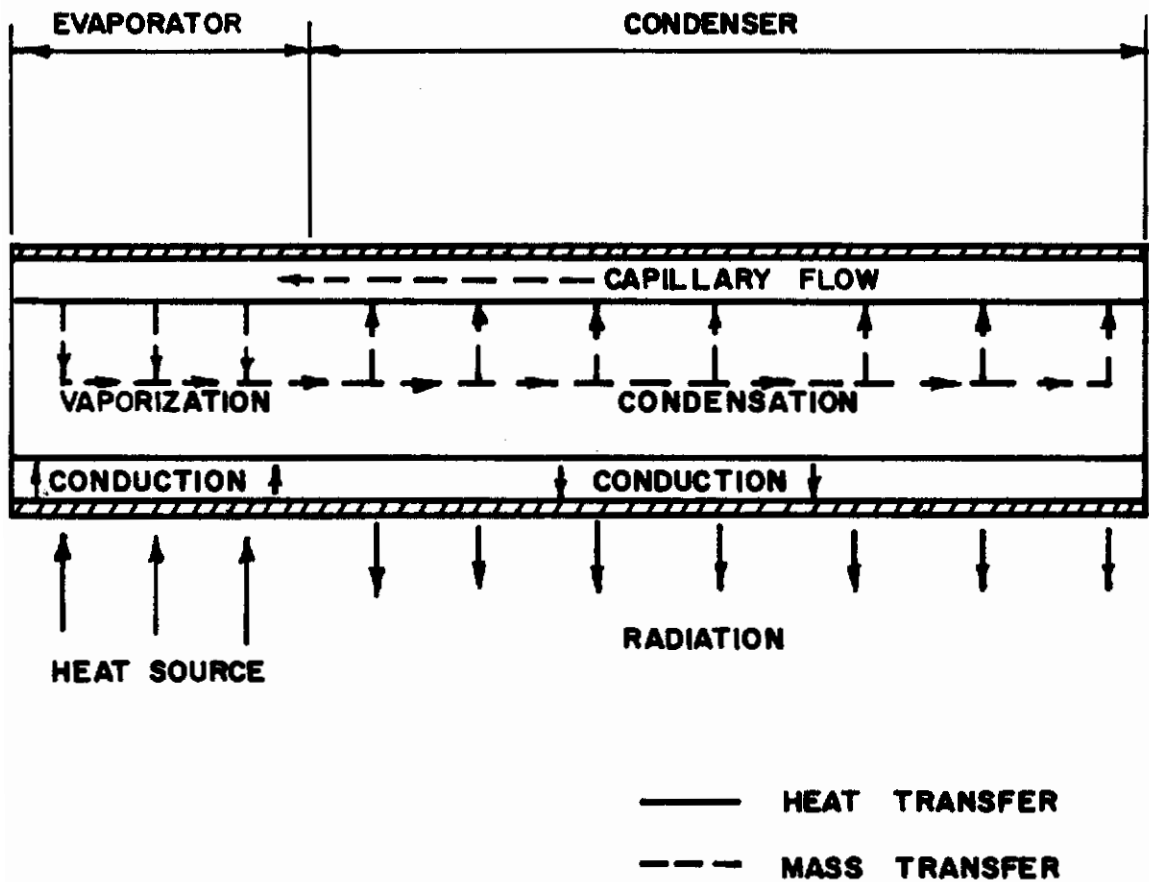
FIGURE 1. HEAT AND MASS TRANSFER IN A HEAT PIPE

The process of transfering heat from the source to the outer surface of the evaporator is, in general, ill-defined. The thermal contact resistance, among other considerations, can vary widely depending on the particular application. For this reason, modeling parameters are not presented for the evaporator section of the heat pipe.

The Modeling Equations

Since the thermal behavior of a heat pipe can be influenced by a variety of conditions, it is important to list the major restrictions and assumptions. They are:

(1) The rejected heat flux is constant over the outer surface of the condenser.

(2) The wick is saturated with liquid, but there is no excess liquid.

(3) There is negligible resistance to mass flow in the heat pipe other than the resistance offered by the wick.

(4) The effects of gravity are negligible.

(5) The thermal conductivity of the liquid saturated wick (in the radial direction) may be represented by a constant.

(6) Heat conduction in the wick and wall, in the axial direction, is negligible compared to heat conduction in the radial direction.

6

(7) The liquid saturated wick and wall interface has
negligible resistance to heat transfer.

(8) Heat transfer inside the wick in the radial direc-
tion, by convection, is negligible compared to
conduction.

(9) The wick pumping capability is limited by capillary
forces and not boiling characteristics.

The vital restriction on heat pipe performance is the
limited output of the capillary pump. This restriction indi-
cates that proper modeling of the wick is of utmost importance
for proper thermal scale modeling.

Since the effects of gravity may be neglected, the wick
offers the only resistance to mass flow from the condenser to
the evaporator. In addition, low flow rates and low velocities
encountered in capillary flow assure that the flow is laminar
and relatively free from inertia effects. For this situation
the empirical relationship knows as Darcy's law will apply (4).
Darcy's equation may be written as

$$\frac{dP}{dx} = \frac{\dot{m}_f \mu_f}{k A_T \rho_f} \qquad (1)$$

where $\frac{dP}{dx}$ is the pressure gradient in the liquid in the direction
of flow, μ_f is the liquid viscosity, ρ_f is the liquid density,
A_T is the total cross-sectional area of the wick perpendicular
to the direction of flow, and $\dot{m}_f$ is the rate of mass transport
at any axial position (x) in the wick. The proportionality

7

constant in this equation, k is the specific permeability of the wick. This permeability constant is a function of wick geometry only. The reciprocal of k is known as the "wick friction factor" and experimental values are available for a variety of wicking materials (4,5).

Non-dimensionalizing Equation (1) results in the dimensionless group

$$(\frac{L\mu_f \dot{m}_T}{P_T k \rho_f A_T})$$ \hfill (2)

where L is a characteristic length associated with the heat pipe, and P_T is the total capillary pumping pressure causing flow through the wick, and $\dot{m}_T$ is the total mass flow rate, which is the flow rate at the evaporator-condenser interface.

The capillary pressure drop, or pumping pressure, is determined from the surface tension of the liquid (σ_f) and the evaporator mean radius of curvature (R) of the menisci. The evaporator mean radius of curvature is the mean radius of curvature of the liquid-vapor interfaces in the evaporator section. The radius of curvature of a liquid-vapor interface located at the far end of the condenser (i.e., the end away from the evaporator) would be large, approaching infinity. Simply stated, the wick should be flooded at the far end of the condenser. Under these conditions the capillary pumping pressure has been shown by Cosgrove et al. (3), to be

$$P_T = \frac{2\sigma_f}{R}$$ \hfill (3)

8

By substitution of equation (3) into (2) there results

$$\left(\frac{LR\mu_f \dot{m}_T}{2\sigma_f k\rho_f A_T} \right) \tag{4}$$

Since the differential equation for the model is the same as the differential equation for the prototype, the dimensionless group (4) must have an identical numerical value for both model and prototype. This means that

$$\frac{\left[\dfrac{LR\mu_f \dot{m}_T}{2\sigma_f k\rho_f A_T} \right]_m}{\left[\dfrac{LR\mu_f \dot{m}_T}{2\sigma_f k\rho_f A_T} \right]_p} = 1 \tag{5}$$

where the subscripts m and p have been used to designate model and prototype characteristics. In order to simplify later equations, starred quantities will hereafter represent the model to prototype ratio of that parameter (i.e., $T* = T_m/T_p$, $q* = q_m/q_p$, etc.). Equation (5) may then be written as

$$\left[\frac{LR\mu_f \dot{m}_T}{\sigma_f k\rho_f A_T} \right]^* = 1 \tag{6}$$

Next, the heat transfer equations for the heat pipe will be considered. Energy transport along the heat pipe is accomplished by convection, and may be expressed as

$$q = \dot{m}_T h_{fg} \tag{7}$$

where q is the total heat transported per unit time and h_{fg} is the latent heat of vaporization of the liquid percolating through the heat pipe.

9

Energy is transported through the wick and wall of the heat pipe by conduction. The energy equation for a series composite tube of two layers is

$$q = \frac{2\pi L_c (T_v - T_o)}{\dfrac{\ln r_2/r_1}{K_1} + \dfrac{\ln r_3/r_2}{K_2}} \qquad (8)$$

where T_v is the temperature of the vapor, T_o is the condenser outer surface temperature, L_c is the condenser length, r_1 is the inner radius of the wick, r_2 is the outer radius of the wick, and r_3 is the radius of the outer condenser surface. K_1 and K_2 are thermal conductivities of the liquid saturated wick and pipe wall, respectively.

Energy transferred away from the heat pipe by radiation to black surroundings at zero degrees Rankine may be expressed as

$$q = \epsilon \sigma_o A_c T_o^4 \qquad (9)$$

where ϵ is the emittance of the condenser surface, σ_o is the Stefan-Boltzmann constant, and A_c is the outer surface area of the condenser.

Since equations (7), (8) and (9) are of the same form for the model and the prototype, there results

$$\frac{q_m}{q_p} = \frac{[L_c(T_v - T_o)]_m}{[L_c(T_v - T_o)]_p} \frac{\left[\dfrac{\ln r_2/r_1}{K_1} + \dfrac{\ln r_3/r_2}{K_2}\right]_p}{\left[\dfrac{\ln r_2/r_1}{K_1} + \dfrac{\ln r_3/r_2}{K_2}\right]_m}, \qquad (10)$$

10

$$\frac{q_m}{q_p} = \frac{(\dot{m}_T h_{fg})_m}{(\dot{m}_T h_{fg})_p} \; , \tag{11}$$

and

$$\frac{q_m}{q_p} = \frac{(\epsilon \sigma_o A_c T_o^4)_m}{(\epsilon \sigma_o A_c T_o^4)_p} \; . \tag{12}$$

These equations are in a dimensionless form and with further simplifications the equations become

$$\left[\frac{L_c(T_v - T_o)}{q(\dfrac{\ln \, r_2/r_1}{K_1} + \dfrac{\ln \, r_3/r_2}{K_2})} \right]^* = 1 \; , \tag{13}$$

$$\left[\frac{\dot{m}_T h_{fg}}{q} \right]^* = 1 \; , \tag{14}$$

and

$$\left[\frac{\epsilon A_c T_o^4}{q} \right]^* = 1 \; . \tag{15}$$

These equations along with the dimensionless grouping derived from the Darcy equation,

$$\left[\frac{L R \mu_f \dot{m}_T}{\sigma_f k \rho_f A_T} \right]^* = 1 \; , \tag{6}$$

comprise the modeling equations for a heat pipe in a cold-wall, high-vacuum environment.

11

Modeling Techniques

Two modeling techniques are presented in this thesis. They are: (1) A model preserving materials, and (2) A model maintaining the same heat flow per unit area.

For thermal scale modeling it is usually assumed that certain of the following items are preserved from prototype to model: Temperature at homologous points; materials at homologous points; heat flux at homologous points; surface finish at homologous points; and scale in each direction. These items are not all mutually exclusive; and combinations of them have been used successfully to make models of relatively simple prototypes (1). In general, the only mutually exclusive criteria are temperature preservation and material preservation at homologous points.

The first modeling technique was chosen for experimental validation because of its distinct advantage over other techniques. Because the wicking material and working fluid are the same in both model and prototype, the modeling equations can be greatly simplified by virtue of thermophysical property considerations.

The similarity relations for the second modeling technique will be presented without experimental verification.

Material Preservation Model

The technique of material preservation will require that the heat pipe wall, wick, and operating fluid be the same for

12

both model and prototype. The wick must also have the same thermophysical properties of porosity, thermal conductivity, etc. Heat pipe length, outside diameter, wall thickness, and wick thickness are assumed to be scaled according to the factor L*.

The emitting surfaces of the prototype and model heat pipes, as well as the surrounding wall of the test chamber, were sprayed with a flat black paint. The paint used was "velvet coating 101-C10," a product of Minnesota Mining and Manufacturing Company, which has been acclaimed to have high uniform values for emittance and absorptance (11).

In accordance with the facts and assumptions presented, the modeling equations can be greatly simplified for the case of material preservation. In this regard, the following characteristics will be considered invariant from prototype to model: (1) the thermal conductivities of the wall and wick, K_1 and K_2, (2) the emittance, ϵ, and (3) the specific permeability, k.

The modeling equations become:

$$\left[\frac{L(T_v - T_o)}{q}\right]^* = 1 , \tag{16}$$

$$\left[\frac{\dot{m}_T h_{fg}}{q}\right]^* = 1 , \tag{17}$$

$$\left[\frac{L^2 T_o^4}{q}\right]^* = 1 , \tag{18}$$

and

13

$$[\frac{R\mu_f \dot{m}_T}{\sigma_f \rho_f L}]^* = 1 , \tag{19}$$

and by rearranging terms and combining equations there results,

$$(T_v - T_o)^* = q^*/L^* \tag{20}$$

$$T_o^* = (q^*)^{1/4}/(L^*)^{1/2} \tag{21}$$

and

$$q^* = (\frac{N}{R})^* L^* . \tag{22}$$

In Equation (22), the group $\frac{\sigma_f \rho_f h_{fg}}{\mu_f}$ has been replaced by N, a liquid parameter. At a specified saturation temperature, the value of N is determined.

The radius of curvature of the liquid-vapor interface R is a function of the local heat flux, the structure or pore size, and the liquid-vapor-solid interfacial free energies. The fact that R is a function of heat flux is easily visualized by noting that increased heat transfer rates cause the liquid in the evaporator to recede into the wick and assume a smaller radius of curvature. This radius is also, of course, a function of pore size. The interfacial free energies determine the wetting characteristics of the wick-liquid combination, and thereby also influence the radius of curvature.

For this modeling technique the liquid (water) and wick (200 mesh nickel wire screen with 67±1% porosity) are the same for both model and prototype. This assures that the pore

14

size is the same for model and prototype, and in addition, it provides increased confidence in reproducible wetting characteristics since only this one wick-liquid combination is used. The usual assumption made in regard to the wetting characteristics is that they are invariant with liquid temperature. In general this assumption is not true. However, over the modest temperature deviations in this experiment work (i.e., 100 F) the assumption may be regarded as true. Experimental data to substantiate this assumption are presented later in this section.

For proper modeling, wick pumping similarity is required. This occurs when the value of the evaporator mean radius of curvature is identical in model and prototype (since temperature and pore size effects are negligible as discussed above). This definition of similarity is justified by considering the capillary pumping parameter $(\frac{k}{R})$, defined by Kunz, which represents the ratio of the capillary forces to the friction forces (5). Wick pumping similarity means that this parameter must be identical for model and prototype, and since the specific permeability k is invariant for this modeling technique, it follows that the evaporator mean radius of curvature R must be invariant.

By virtue of all the above considerations it is required (for proper thermal scale modeling) that

$$R^* = 1 . \tag{23}$$

By substitution into Equation (22), there results:

$$q^* = N^*L^* \tag{24}$$

15

Equations (20), (21), and (24) are in a form suitable for calculations and may be used to predict prototype thermal behavior.

Heat Flux Preservation Model

For heat flux preservation the only quantities that are identical for model and prototype are the heat flux (q/L^2) and emittance (ϵ). Combining and rearranging Equations (6), (13), (14), and (15) there results

$$\left[\frac{(T_v - T_o)}{L\left(\dfrac{\ln\, r_2/r_1}{K_1} + \dfrac{\ln\, r_3/r_2}{K_2}\right)}\right]^* = 1 , \tag{25}$$

$$\left(\frac{LR}{kN}\right)^* = 1 , \tag{26}$$

and

$$(T_o)^* = 1 . \tag{27}$$

No further reduction of these modeling equations may be made without consideration of the specific materials involved.

It is interesting to note that the skin temperature of the condenser has been preserved by this modeling technique. As a result, temperatures throughout the model and prototype will be very nearly equal and the water parameter N will also be approximately preserved.

Discussion of Assumptions

The assumptions, listed earlier in this section, will be discussed in the same order as originally presented.

The first assumption concerning constant heat flux was shown experimentally to be valid. Since the heat pipe operated at nearly constant temperature over the surface of the condenser (the maximum deviation was 9° F and occurred at the evaporator-condenser interface) the radiant energy flux may then be assumed constant.

It is not apparent what shape the liquid-vapor interface will assume in the evaporator at high values of heat input. For this reason, the second assumption is not strictly true. Although the condenser section of the wick would be expected to be saturated with liquid at all times, the evaporator liquid-vapor interface will recede into the wick at high values of heat input. A technique used by other investigators to minimize this effect, is to make the evaporator section short compared to the condenser section so that the axial pressure drop in the liquid in the evaporator may be neglected (5). This technique was adopted. Also, the heat pipe was charged with 5% more liquid than needed to completely fill the wick.

Assumption 3 indicates that the vital limitation to mass flow in the heat pipe is the capillary pump or wick. The only two phenomena that would result in the breakdown of the vaporization-condensation cycle are vapor-blockage of the wick and/or insufficient capillary forces to supply sufficient

17

condensate to the evaporator. A few exceptional circumstances could be imagined that would limit mass flow, such as contamination or blockage of the vapor passage, but these were not present in this study. To prevent vapor blockage of the wick by film-boiling, the radial heat in-flux was held below values normally associated with this phenomenon. Experimental evidence that failure of the capillary pump was responsible for limiting heat pipe operation is provided in the results. By these considerations, assumptions 3 and 9 are considered sound.

The effect of gravity was negligible because the heat pipe was horizontally oriented and had small vertical dimensions (i.e., 2 inches). This substantiates assumption 4.

The thermal conductivity of a liquid saturated wick (the subject of assumption 5) has been studied by Gorring (7). Over the temperature range of this experimental investigation the thermal conductivity of saturated liquid water varies from 0.380 to 0.396 Btu/(hr)(ft)(deg F) and the thermal conductivity of nickel varies from 34.5 to 33.0 Btu/(hr)(ft)(deg F). These variations are very small and the thermal conductivity of both the liquid saturated wick and the wall of the container were treated as constant.

Assumption 6 required negligible heat conduction in the axial direction. From measured temperatures, the rate of heat transfer by conduction across the evaporator-condenser interface and radiated away from the condenser surface, was

found to be less than 1/2% of the total energy transferred by the heat pipe.

To provide good interfacial conductance at the liquid-wall, liquid-wick, and wick-wall interfaces, a fluid was selected that wet both the wick and the shell of the heat pipe, and the nickel wick was sintered to the wall of the heat pipe.

Assumption 8 concerns heat transfer by convection in the radial direction inside the wick. This heat transfer is negligible because the liquid in the wick has a negligible radial velocity due to the absence of a radial pressure gradient.

Assumption 9 was discussed with assumption 3.

2. EXPERIMENTAL STUDY

To verify the first modeling technique developed in Section II, two heat pipes (one model and one prototype) were fabricated from identical materials. The second modeling technique, heat flux preservation, was not experimentally investigated.

To corroborate the results of the theoretical analysis, two types of experiments were undertaken. The first involved the construction of a high vacuum, cold wall chamber with support equipment sufficient to measure the characteristics indicative of thermal behavior. The second involved a separate study of certain wick characteristics.

No attempt was made to drive either heat pipe to maximum output while installed in the vacuum chamber. Excessive temperatures and, more importantly, excessive pressures prevented this particular test. As a consequence, wick validation tests (i.e., driving the wick to failure) were performed under more suitable heat transfer conditions.

Heat Pipe Fabrication

One experimental prototype and one experimental model were constructed for the purpose of providing reproducible and reliable information about their operating characteristics. The general configuration is illustrated in Figure 2.

20

NICKEL SCREEN WIRE WICK
200 SQUARE MESH

NICKEL PIPE WALL

HEAT PIPE DIMENSIONS
(INCHES)

MODEL

r_1 = 0.352

r_2 = 0.412

r_3 = 0.486

L = 6.12

PROTOTYPE

r_1 = 0.667

r_2 = 0.802

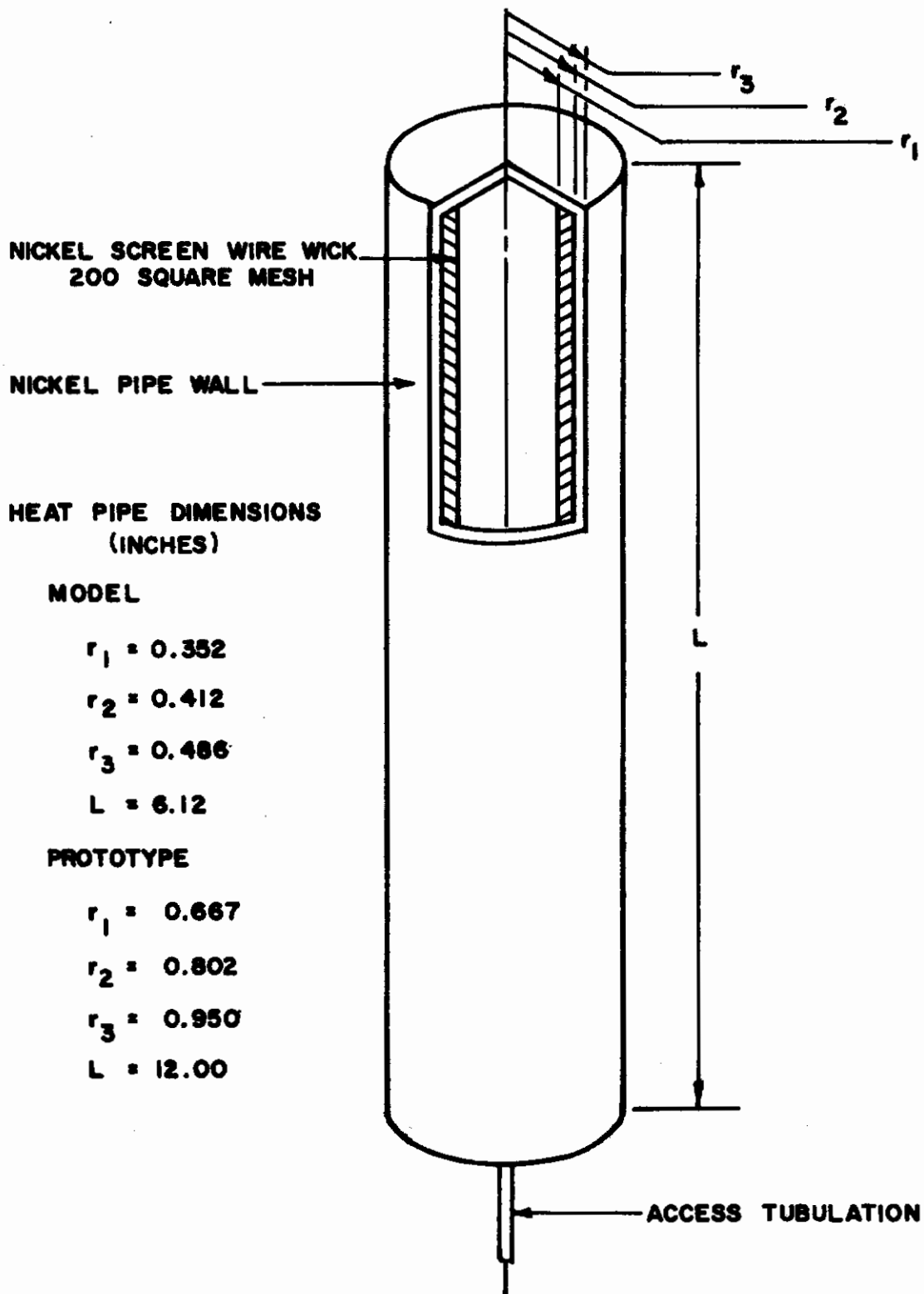r_3 = 0.950

L = 12.00

r_3

r_2

r_1

L

ACCESS TUBULATION

FIGURE 2. OVERALL DIMENSIONS

21

Both units were constructed from nickel pipe and nickel screen wire. The shell of the model and prototype heat pipes were constructed from 3/4" and 1 1/2" IPS nickel pipe respectively. By machining only one surface, the outer surface of the 3/4" IPS pipe, a dimensional scale factor $L^* = 0.512$ was established.

The porous wicks were formed by coiling 200 mesh nickel screen wire into a continuous coil. This multilayer coil was pressed against the inside wall of the nickel pipe and sintered in a furnace with an ammonia atmosphere. A similar procedure was used by Kunz (5).

The wick porosity (the total pore volume of the wick divided by the total wick volume) was determined by calculating the total volume of wire used in making the wicks and by measuring the dimensions of the finished wick. The calculated porosities of both wicks agreed, within 1%, with the value experimentally measured (67.6%) by Kunz (5). This indicates that the wick structures are indeed comparable.

The dimensions obtained during or after fabrication are listed in Figure 2. Although the scaling factor was $L^* = 0.512$, not all the final dimensions were in this ratio. Some geometrical distortion was introduced because of fabricational difficulties. Because of these slight deviations from similarity the modeling equations were altered to reflect dimensional distortion.
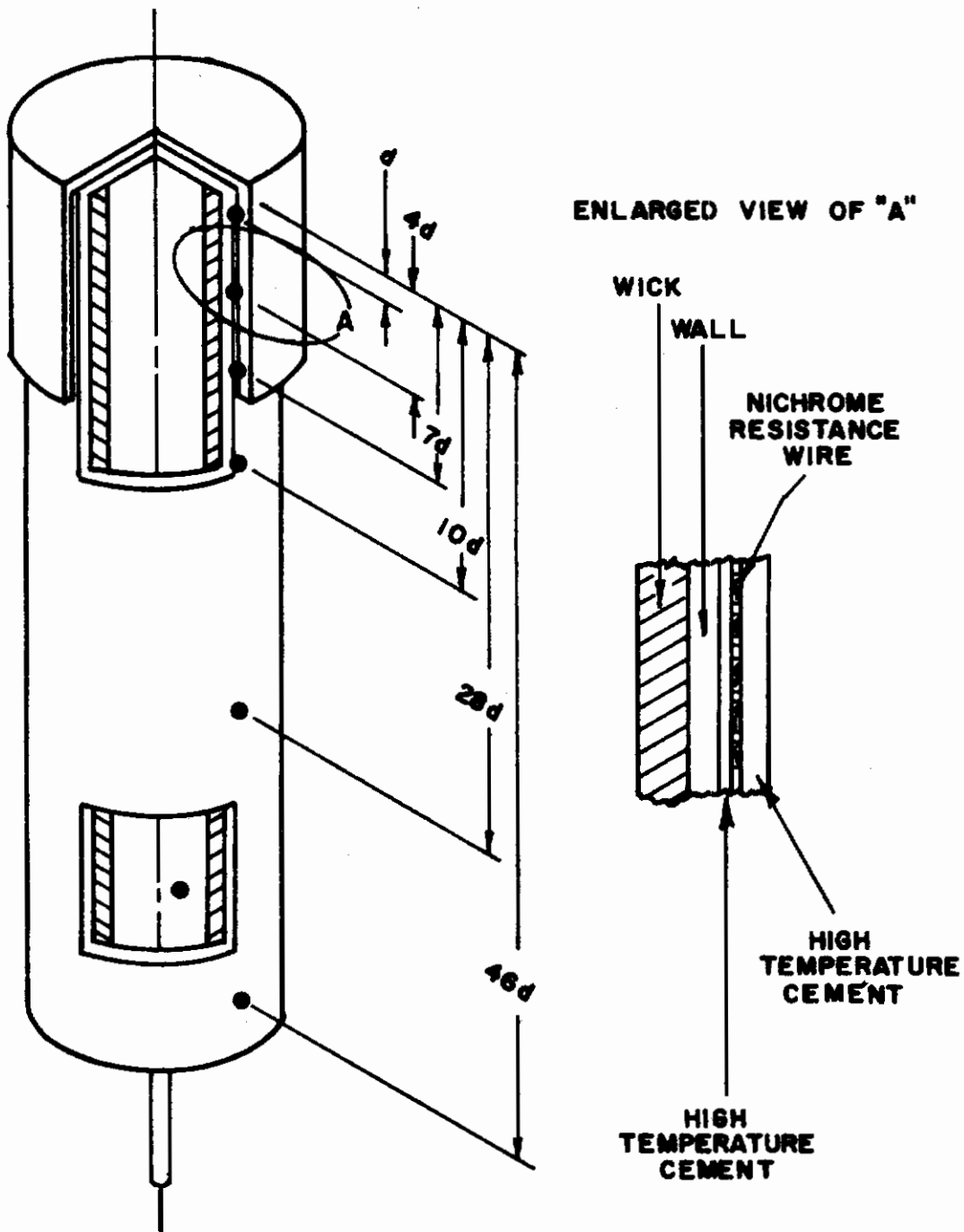
22

Heat Pipe Preparation

A 30 gage copper-constantan thermocouple was installed inside the vapor cavity as illustrated in Figure 3. The heat pipe was then connected to a vacuum pumping station, as shown in Figure 4, and leak checked. No measurable leakage was found through the model or the prototype at a pressure of 2×10^{-6} torr.

Contaminants were driven from the cavity of the heat pipe by a vacuum bake-out operation. While the pressure was maintained below 2×10^{-5} torr; the temperature of the heat pipe was increased to 500°F. At the conclusion of this degassing operation, and without breaking the vacuum on the heat pipe deionized, distilled, and degassed water was allowed to enter the heat pipe in an amount sufficient to fill the wick with liquid and the vapor cavity with vapor. The heat pipe tubulation was pinched closed and rechecked for leakage through the pinched tubulation. No leakage was detected from either heat pipe at pressure levels as low as 2×10^{-6} torr, so the tubulation was severed and permanently sealed with silver solder.

Instrumentation for Cold Wall, High Vacuum Tests

Twelve 30 gage copper-constantan thermocouples were welded to the outer surfaces of the heat pipes as shown in Figure 3. The thermocouples were located at homologous positions on model and prototype.

ENLARGED VIEW OF "A"

WICK

WALL

NICHROME
RESISTANCE
WIRE

HIGH
TEMPERATURE
CEMENT

HIGH
TEMPERATURE
CEMENT

d — 1/4 INCH FOR PROTOTYPE AND 1/8 INCH FOR MODEL

● — THERMOCOUPLE LOCATIONS (POSITIONS 180° OPPOSED NOT SHOWN)

FIGURE 3. INSTRUMENTED HEAT PIPE

GRADUATED
CYLINDER

CASCADE REFRIGERATION
SYSTEM FOR COOLING
A 6 INCH COLD TRAP

HIGH VACUUM
PUMPING STATION
WITH
IONIZATION GAGE
6" SLIDE VALVE
6" COLD TRAP
6" OIL DIFFUSION PUMP
MECHANICAL ROUGHING PUMP
MECHANICAL HOLDING PUMP

HEAT PIPE

OVEN POSITION

AC POWER SUPPLY

OVEN

HAND BALANCED
MILLIVOLT
POTENTIOMETER
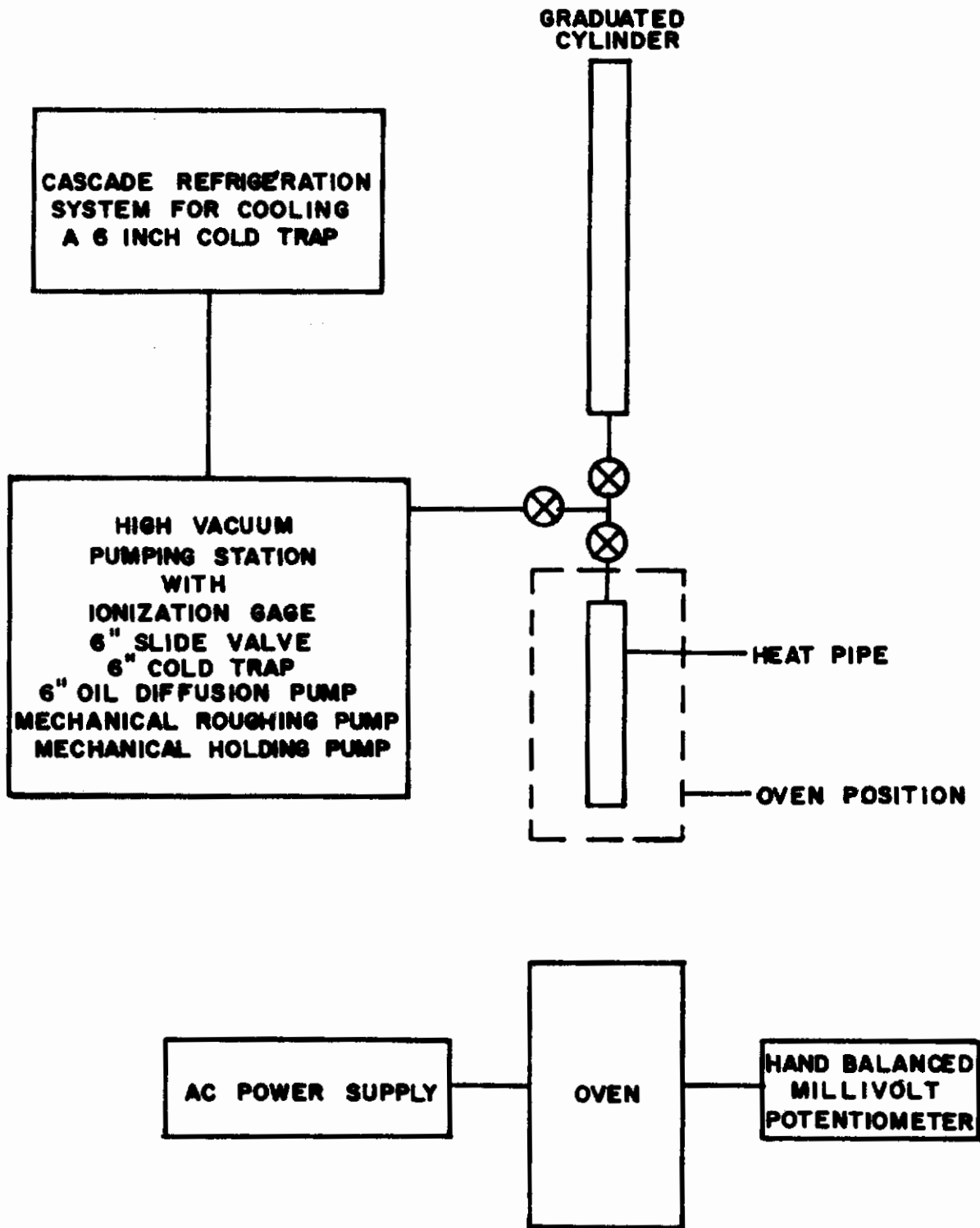
FIGURE 4. PREPARATORY SYSTEM

25

A thin coat of Sauereisen adhesive cement (manufactured by the Sauereisen Cements Company) was applied to the evaporator section of the heat pipes to isolate the metalic heat pipes from the electrical heaters. Nichrome ribbon was wrapped tightly over this adhesive cement and secured in place by additional coatings of cement. The finished heater was wrapped with several layers of aluminum foil to provide a radiation shield.

Electrical resistance heating was provided by the nichrome ribbon. A regulated D.C. power supply was used to supply electrical power, and the power input was determined by using a voltmeter and ammeter as shown in Figure 5. A hand-balanced millivolt potentiometer was used to measure thermocouple output.

Cold Wall, High Vacuum Chamber

The test chamber for space cold wall, high vacuum is illustrated in Figure 6.

A high vacuum oil diffusing pumping station fitted with an 18" bell jar was used to create a vacuum environment. Pressures during all tests were observed to be less than 1×10^{-6} torr, as indicated by a hot filament ionization gage. Another heat pipe leak check was obtained by measuring the ultimate pressure of the vacuum system before and after heat pipe installation. Again, no measurable leakage was observed.

A liquid nitrogen cold wall was formed by coiling 3/8" copper tubing around a 4" diameter mandrel to an overall length

26
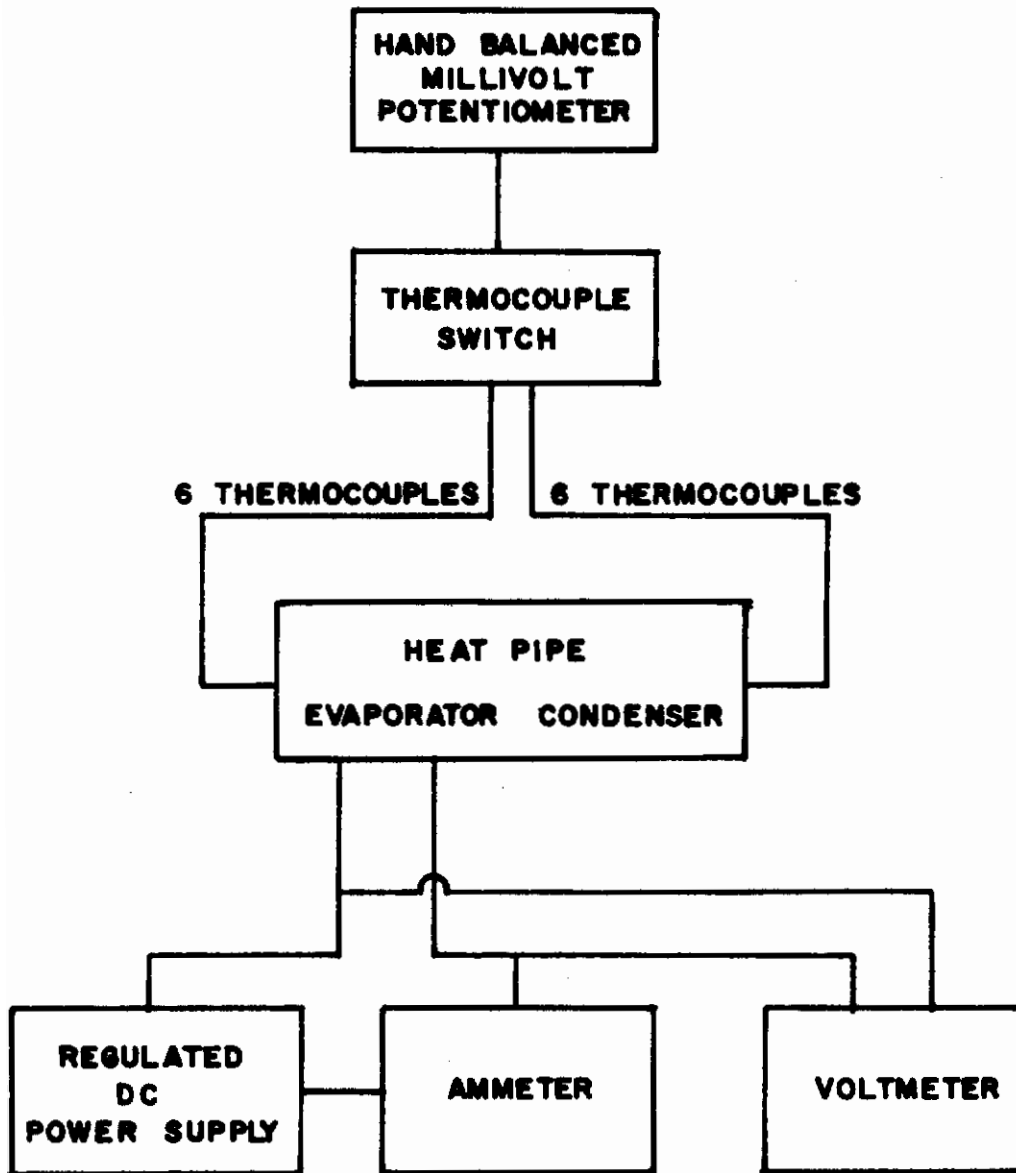
FIGURE 5. INSTRUMENTATION FOR SPACE SIMULATION TESTS

18 INCH DIAMETER BELL JAR

LIQUID NITROGEN COIL

HEAT PIPE

LIQUID
NITROGEN
OUT

LIQUID
NITROGEN
IN

HIGH VACUUM
PUMPING STATION
WITH
4" SLIDE VALVE
4" COLD TRAP
4" OIL DIFFUSION PUMP
MECHANICAL PUMP

FEED-THROUGH
FOR
DC POWER

FEED-THROUGH
FOR 20
COPPER-CONSTANTAN 30
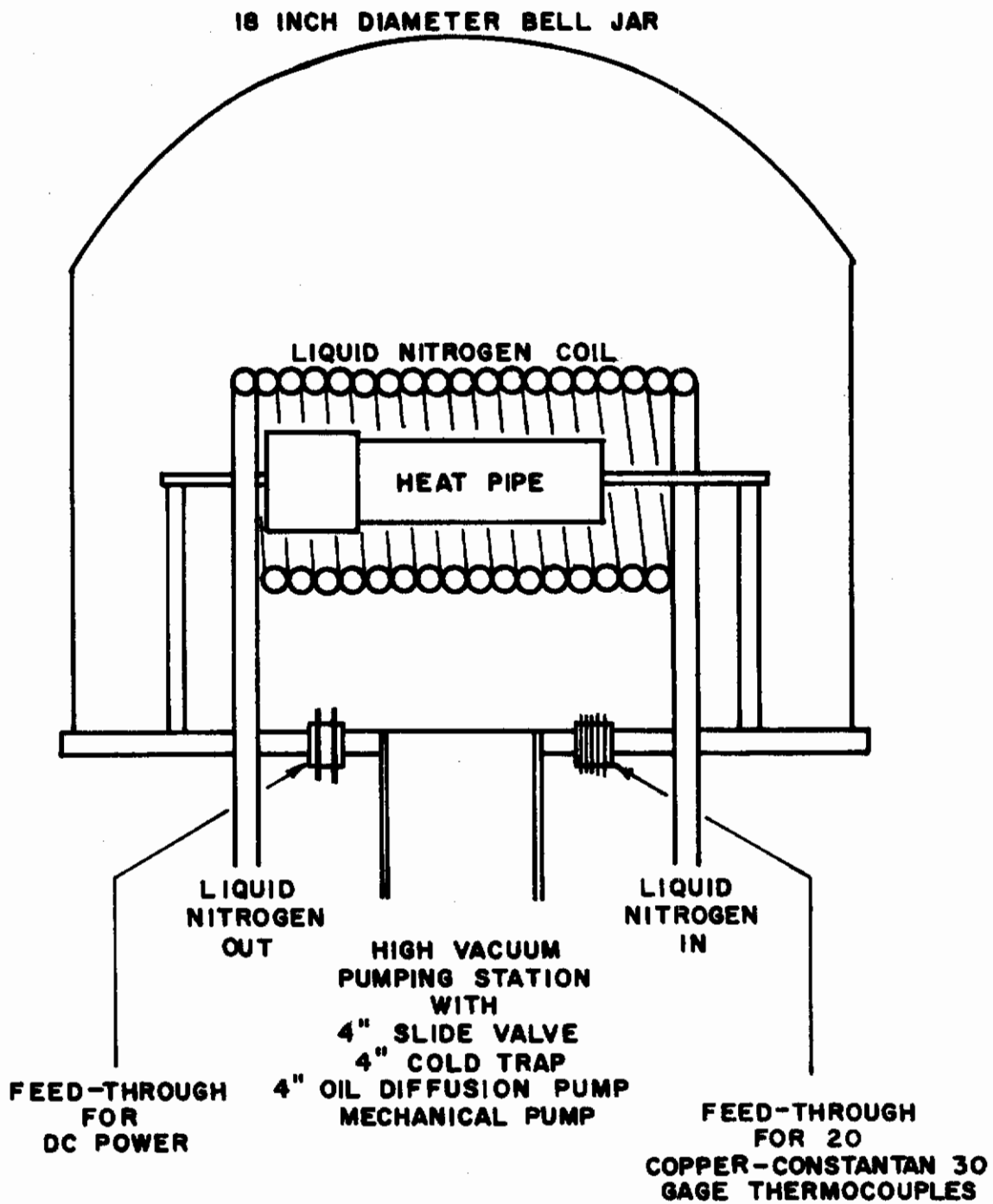GAGE THERMOCOUPLES

FIGURE 6. SPACE SIMULATION CHAMBER

28

of 14". The individual coils were secured to one another by silver solder, so the resulting wall was optically dense in the radial direction. The inner surface of the liquid nitro- gen jacket, like the condenser surface of the heat pipe, was sprayed with flat black paint.

Procedure for Cold Wall, High Vacuum Tests

With the heat pipe carefully installed inside the simula- tion chamber, tests were started by activating the high vacuum pumping station. Pressures were generally below 2×10^{-5} torr in less than an hour. Thermocouples were monitored to assure uniformity of output under conditions of thermal equilibrium and no heat input. Liquid nitrogen was admitted to the cold wall tubulation and allowed to flow until the entire coil was at liquid nitrogen temperature. At the same time, power was supplied to the test sample to prevent the liquid inside the heat pipe from freezing.
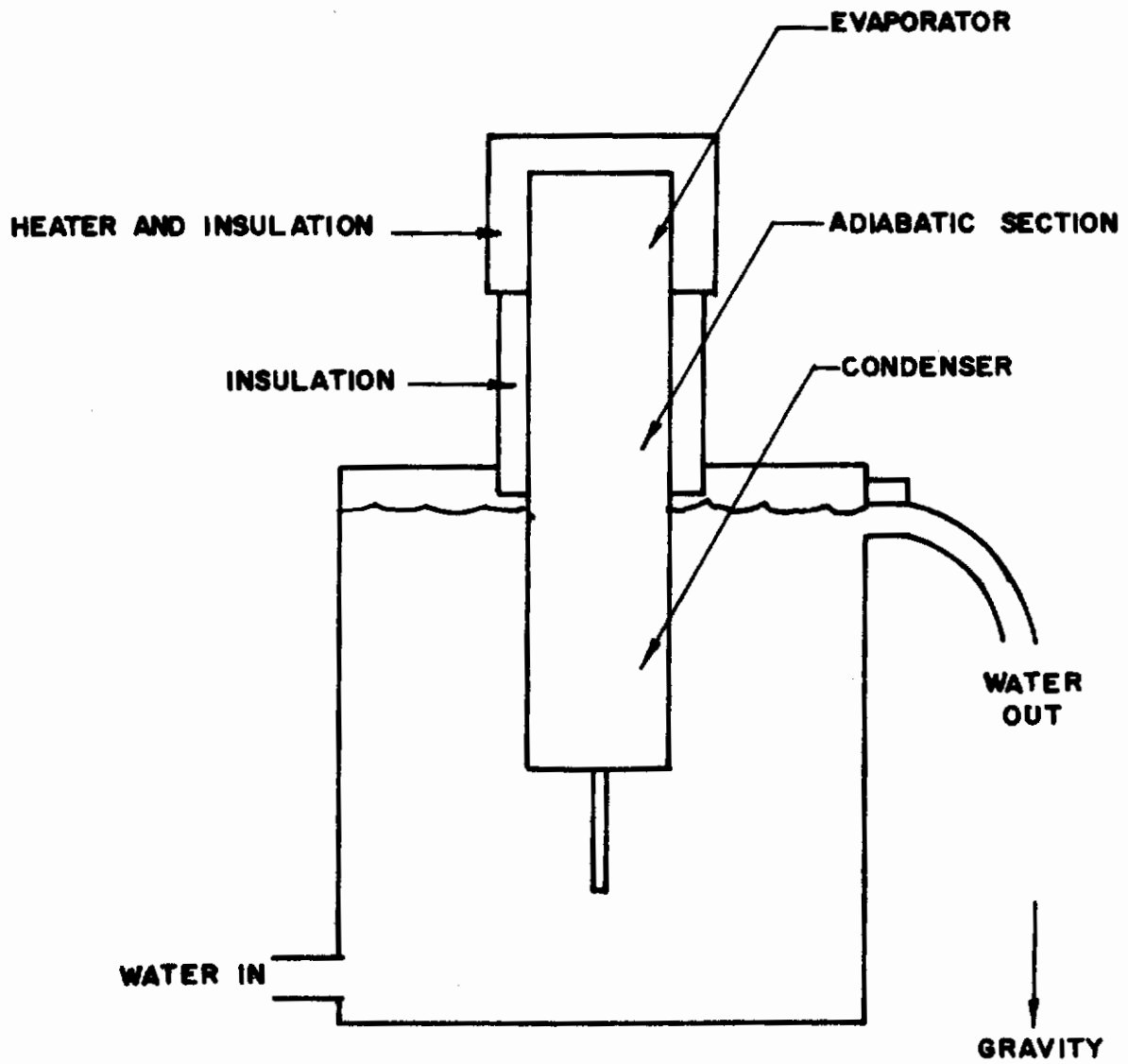
While liquid nitrogen circulated continuously through the coil, the voltage drop across the heater was varied to obtain the desired heat flux at which data were to be taken. When equilibrium conditions were achieved, that is, when temperatures varied less than $0.8°$ F per hour, the input voltage and current were recorded along with thermocouple outputs. Other recorded measurements pertaining to the environmental conditions were the liquid nitrogen coil temperature and the vacuum system pressure.

After recording all necessary data, the power input was adjusted to another selected value and temperatures and times were recorded at intervals until a new thermal equilibrium was reached.

Wick Pumping Tests

To investigate the pumping capabilities of the wick, both heat pipes were tested by a scheme illustrated in Figure 7. The heat pipes were vertically oriented, working against gravity (i.e., evaporator over condenser), with their condensers submerged in a constant temperature water bath. For these tests an adiabatic section was created by insulating the surface of the heat pipe between the condenser and evaporator. By varying the depth of immersion into the water bath from test to test, heat pipe failure could be made to occur at various internal vapor temperatures (i.e., the greater the depth of immersion, the lower would be the corresponding vapor temperature at heat pipe failure).

In conducting this experimentation only four measured variables were necessary: (1) the base (or root) temperature measured on the surface of the heat pipe and next to the end of the heater, (2) the vapor temperature, (3) the heat input, and (4) the depth of condenser immersion. To obtain these measurements the heat pipes were instrumented as shown in Figure 8.

FIGURE 7. WICK TESTING APPARATUS

31

● THERMOCOUPLE LOCATIONS

3 THERMOCOUPLES LOCATED 120° APART

ENLARGED VIEW OF "A"

WICK

WALL

NICHROME
RESISTANCE
WIRE

A

TIGHTLY
BOUND
WIRE

20 SHEETS
OF MICA

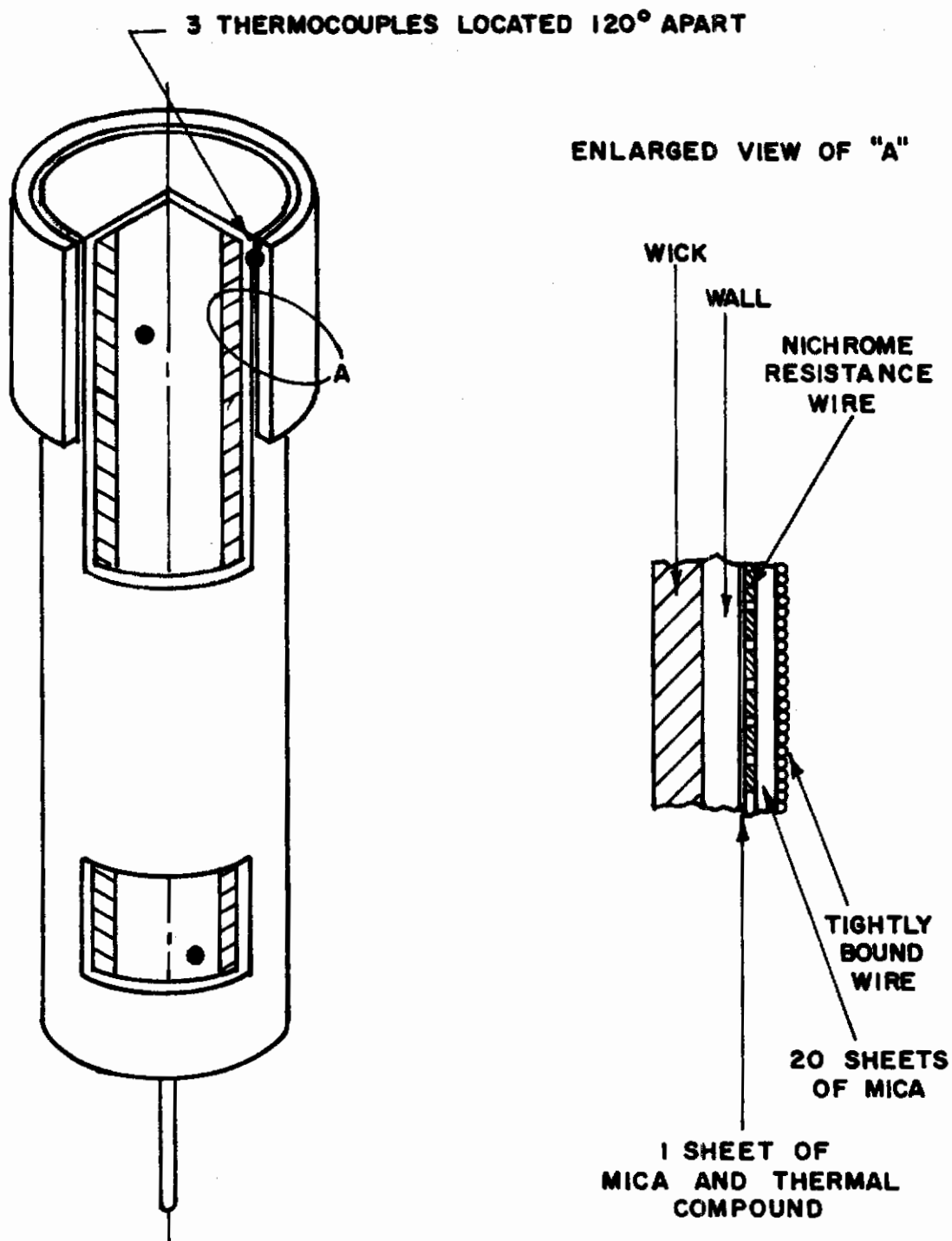1 SHEET OF
MICA AND THERMAL
COMPOUND

FIGURE 8. INSTRUMENTED HEAT PIPE FOR WICK PUMPING TESTS

32

Three 24 gage thermocouples were welded to the end of the heat pipe adjacent to the last coil of the electrical resistance heater. Two 24 gage thermocouples were inserted into the vapor cavity.

A sample heater assembly is illustrated in Figure 8. To provide minimum thermal resistance between the resistance heating element and the surface of the evaporator, the following construction was used:

(1) A Thermal Compound Number 122, manufactured by Wakefield Engineering, Inc., was smeared over the surface of the evaporator to reduce the interfacial thermal contact resistance.

(2) One thin sheet of mica (0.0006 of an inch thick) was placed over the thermal compound and over-wrapped with the nichrome ribbon heating element.

(3) The heater was covered with several more layers of mica and then very tightly secured with wire.

The support equipment used for monitoring input and output variables from the instrumented heat pipe are illustrated in Figure 9. An A.C. power supply was used to provide electrical resistance heating. The inductive losses were shown to be immeasurably small (i.e., less than 1/2 of one per cent error) by an A.C.-D.C. comparison test.

The thermocouple output was monitored on a hand-balanced millivolt potentiometer and the power input was measured with a wattmeter.
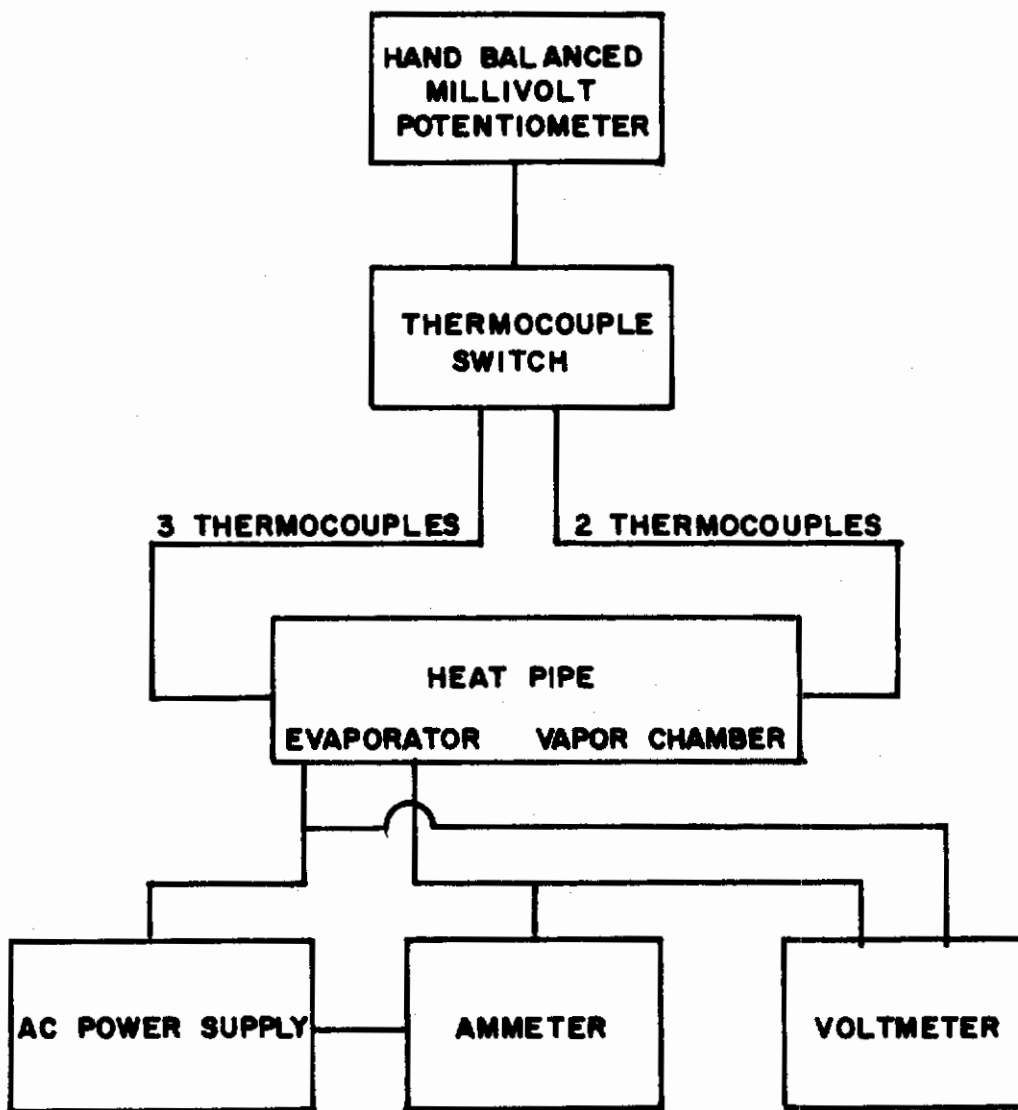
FIGURE 9. INSTRUMENTATION FOR WICK PUMPING TESTS

Procedure for Wick Pumping Tests

To evaluate wick pumping characteristics, the heat pipe was vertically oriented and the condenser end immersed in tap water to a prescribed depth. The vat of tap water was continuously supplied with new tap water serving to maintain constant water level and water temperature.

A wick pumping test was accomplished by slowly increasing the power input by increments until the heat pipe ceased to function properly (i.e., high root temperatures caused by insufficient liquid in the evaporator). The time allotted between incremental input changes was one hour. This was more than enough time to establish thermal equilibrium. After equilibrium was achieved, all necessary data were recorded.

3. RESULTS

The test results for this study were accumulated from 14 experiments; including cold wall, high vacuum tests, wick pumping tests, and replication tests. The results provided by the replication tests were used to check the consistency of the test data. The Fahrenheit temperatures measured in the cold wall, high vacuum tests were reproducible to within 1% and the temperatures from the wick pumping tests to within 5%.

Cold Wall, High Vacuum Tests

Dimensional distortion was encountered in the fabrication of test samples. Consequently, the modeling Equations (20), (21), and (24) had to be altered to reflect the distortion. The equations (which are developed in the appendix) become:

$$(T_v - T_o)^* = q^* A_T^* / (L^*)^3 , \qquad (28)$$

$$T_o^* = (q^*)^{1/4} / (L^*)^{1/2} , \qquad (29)$$

and

$$q^* = N^* A_T^* / L^* . \qquad (30)$$

Note that the dimensionless area of the wick A_T^* cannot be treated as $(L^*)^2$ since distortion was present in the wick.

The results of the space simulation tests are shown in Figures 10 and 11. Model test data were scaled and used to
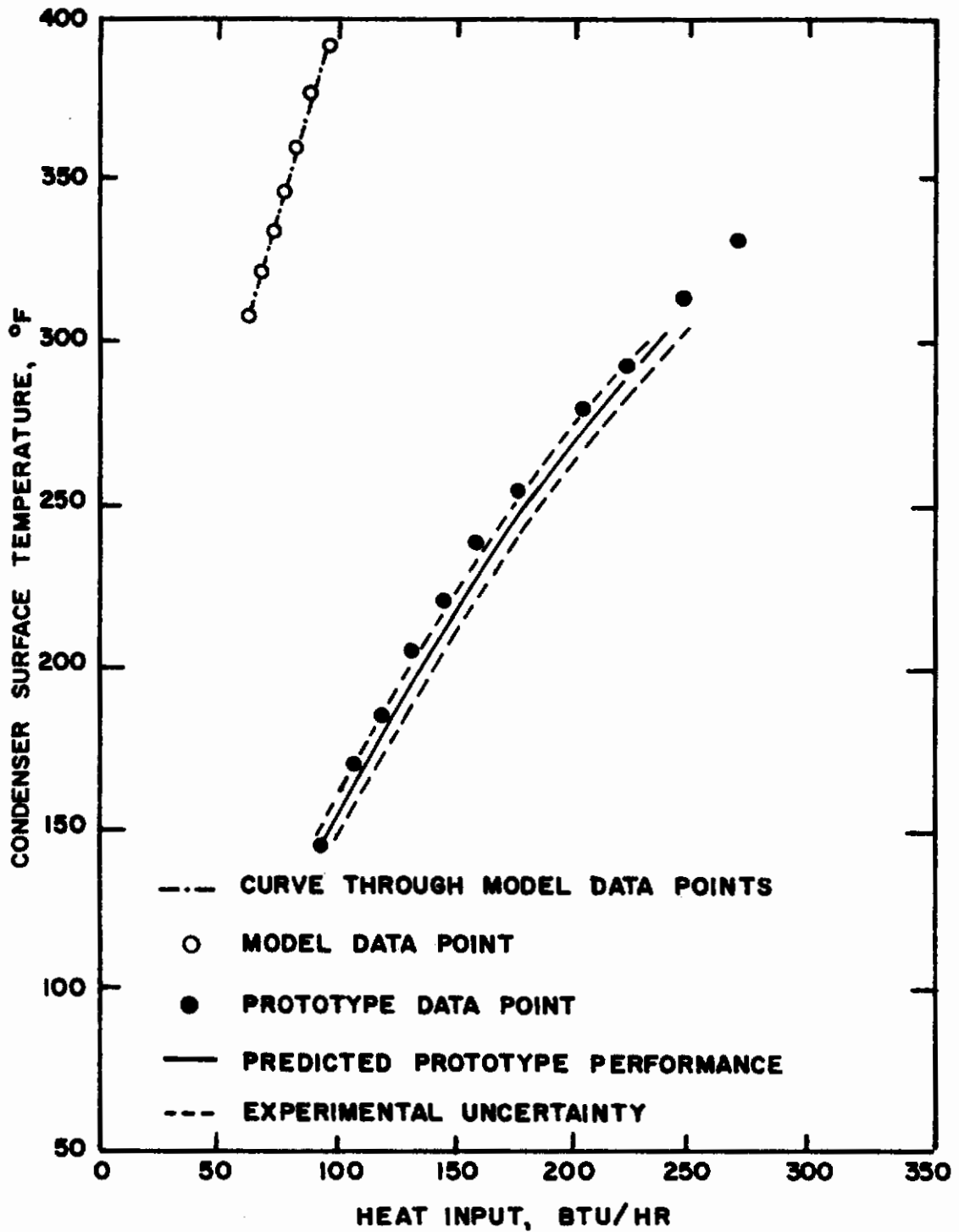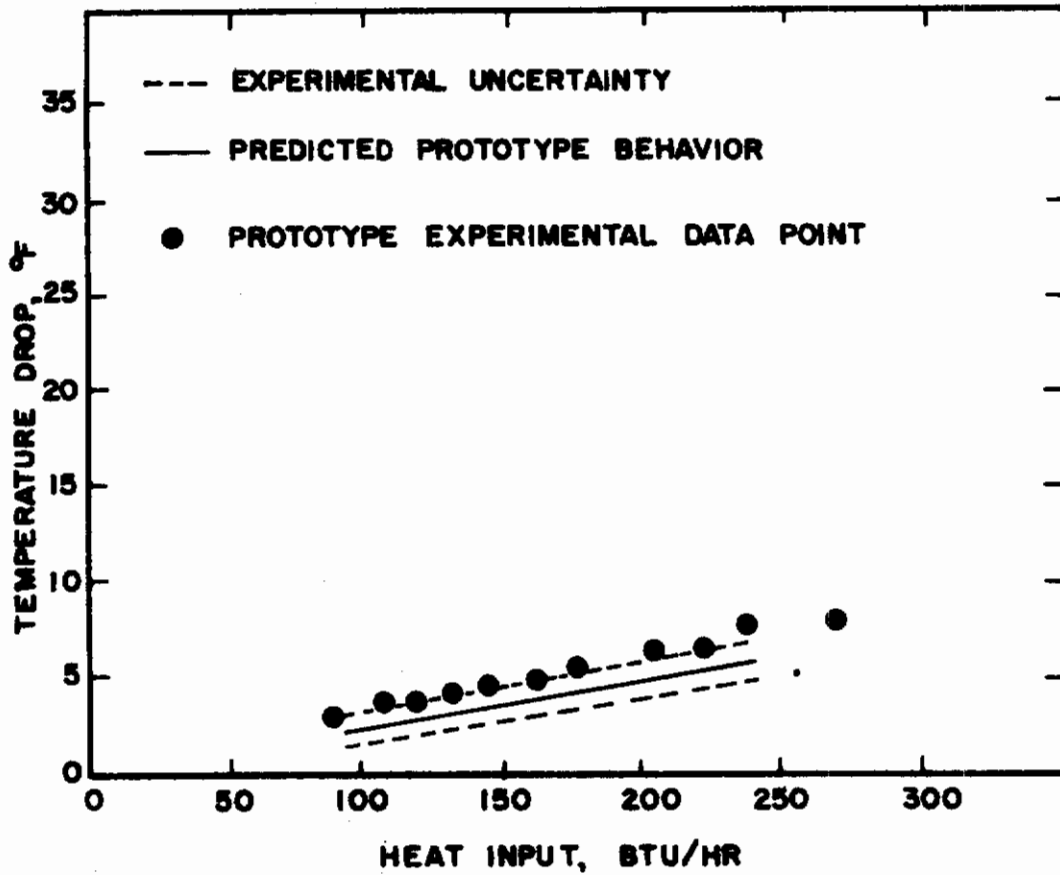
36

FIGURE 10. PREDICTED AND MEASURED PROTOTYPE
CONDENSER SURFACE TEMPERATURE

37

FIGURE II. PREDICTED AND MEASURED PROTOTYPE
TEMPERATURE DROP THROUGH THE
CONDENSER WALL AND WICK

38

predict the thermal behavior of the prototype. This prediction is represented by a smooth curve. Plotted points represent the experimentally measured behavior.

The specific test results for the prototype and model are given in Tables 1 and 2.

Excellent agreement was obtained between predicted and actual prototype behavior. No predicted temperature was more than 10°F in error. Figures 10 and 11 illustrate this fact and also call attention to experimental uncertainties.

Error Analysis for Cold Wall, High Vacuum Tests

The greatest source of error in these experiments was caused by the transport of heat away from the heater by thermocouple wires and power leads. To bound these lead wire losses, the following extremes were considered:

(1) Black lead wires radiating to 0°R and black surroundings.

(2) Leads with $\epsilon = 0.5$, radiating to room temperature surroundings.

Figures 12 and 13 illustrate the extremes for lead wire losses in the prototype and model heat pipes respectively. At a given heater temperature, the distance between these bounding curves is a measure of uncertainty.

End losses by radiation were evaluated for both heat pipes. Because of the well defined geometry and surface conditions, the uncertainty in end losses was one order of magnitude smaller than the uncertainty in the lead wire losses,

39

TABLE I

Measured Prototype Behavior

Heat input (Btu/hr)	Condenser surface temperature[1] (°F)	Temperature drop across the wall (°F)
90	144	3.2
108	171	3.7
120	187	4.0
133	204	4.3
147	222	4.7
163	238	5.0
179	254	5.6
206	280	6.4
224	292	6.7
248	313	7.7
271	330	8.4

[1]The average of four measured surface temperatures, none of which deviated more than 3 °F from this average value.

TABLE II

Experimentally Measured and Thermally Scaled Model Behavior

| Measured Model Data			Model/Prototype Ratios			Predicted Prototype Data		
Heat input (Btu/hr)	Temperature drop across the wall (°F)	Condenser surface temperature (°F)	q^*	T_o^*	$(T_v-T_o)^*$	Heat input (Btu/hr)	Temperature drop across the wall (°F)	Condenser surface temperature (°F)
62.8	2.8	307	0.671	1.26	1.137	94	2.4	146
68.0	2.4	321	0.540	1.20	0.915	126	2.6	191
72.4	2.7	333	0.495	1.17	0.838	145	3.2	216
77.9	3.2	347	0.465	1.16	0.788	168	4.0	238
83.3	2.7	360	0.444	1.14	0.752	188	3.6	258
90.5	3.0	377	0.420	1.13	0.712	215	4.2	284
97.3	4.7	392	0.407	1.12	0.690	239	6.8	303

41
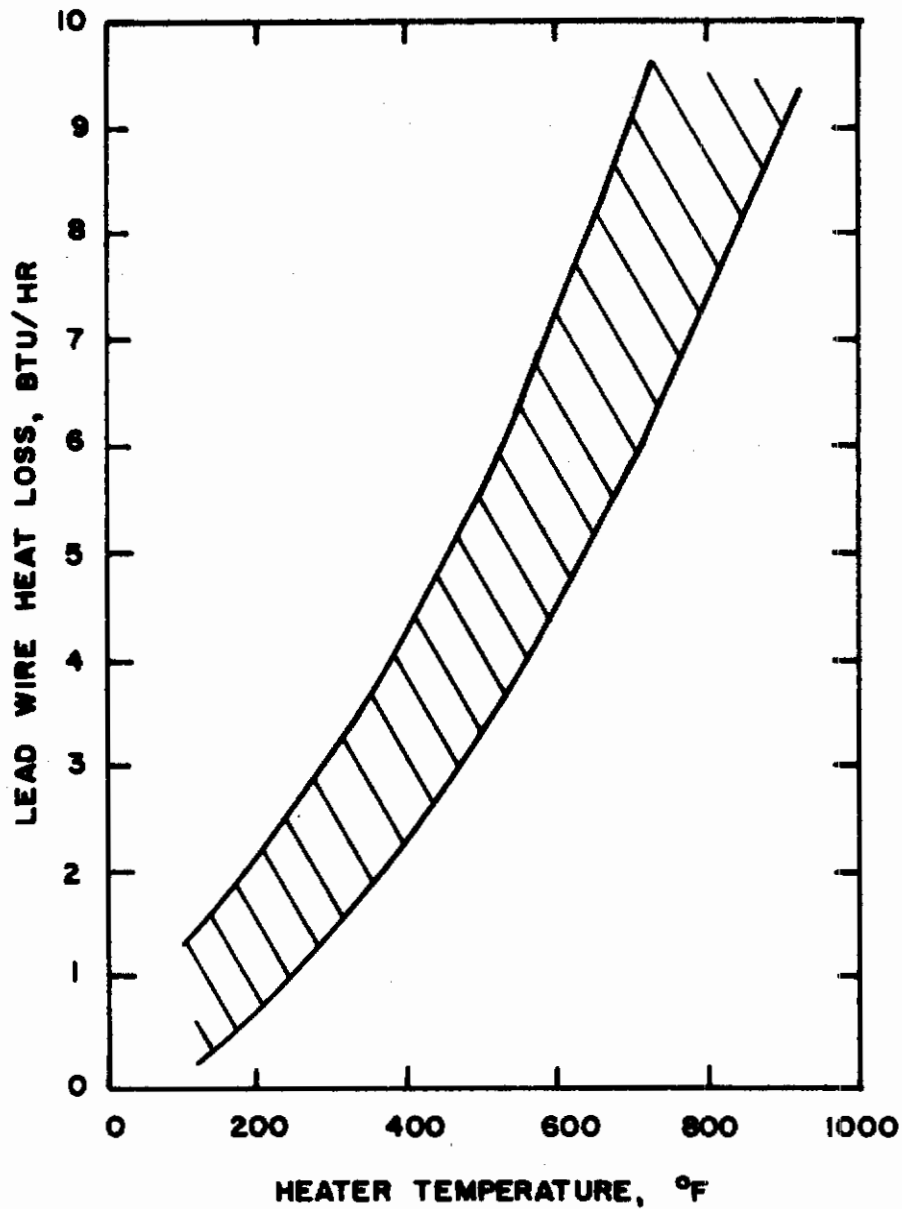
FIGURE 12. UNCERTAINTY BOUND FOR THE LEAD WIRE
HEAT LOSS IN THE PROTOTYPE
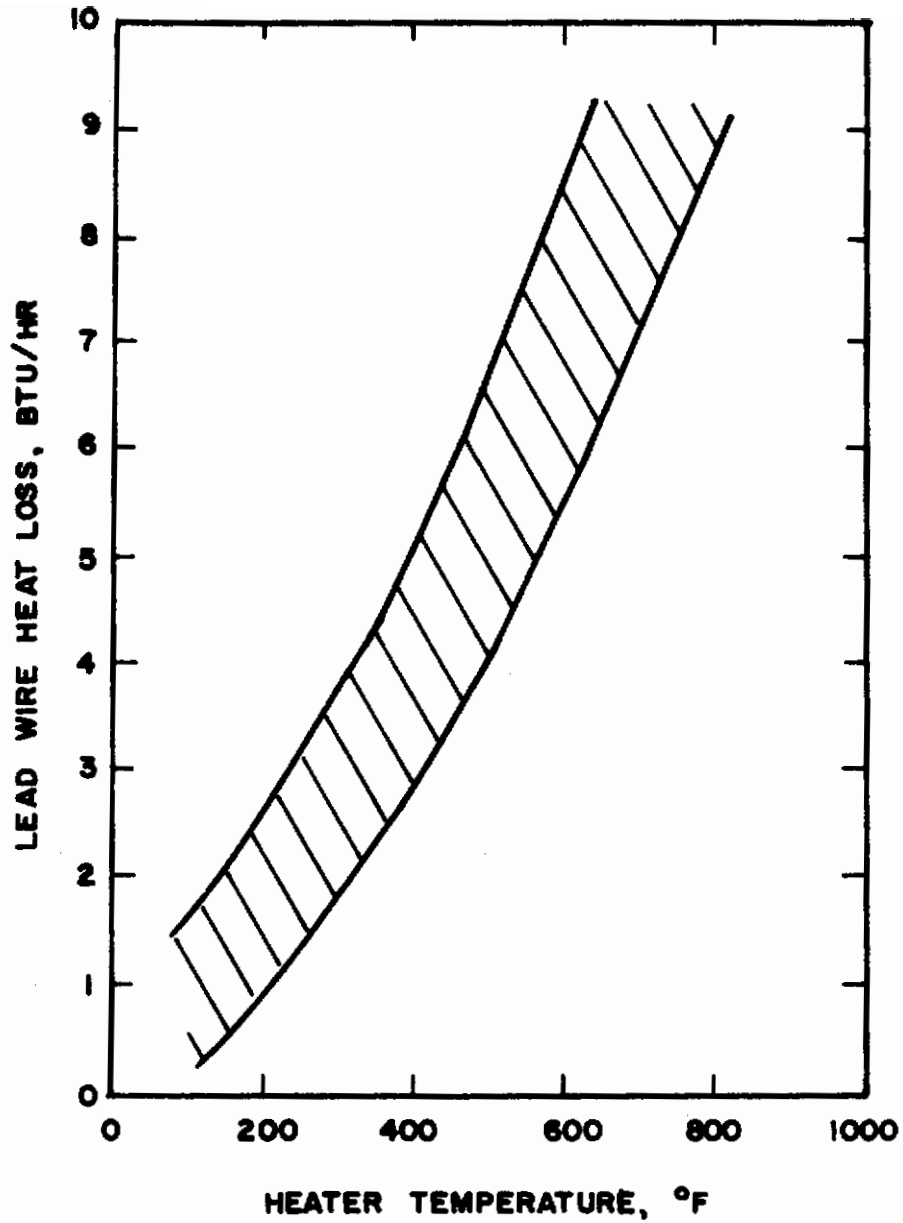
FIGURE 13. UNCERTAINTY BOUND FOR THE LEAD WIRE
HEAT LOSS IN THE MODEL

43

and was neglected. The magnitude of the end loss was not ne-
glected.

Other losses were insignificant compared to above losses.
Heat conduction down the wall was shown to be one of these
insignificant losses. Figs. 14 and 15 show the axial temper-
ature gradients in the walls of the heat pipes. Calculations
from these gradients indicate that even though as much as 5%
of the total heat input crossed the evaporator-condenser inter-
face, only a tenth of this amount was radiated from the con-
denser. The balance of this energy was transferred to the
wick and liquid. Overall, the axial conduction errors were less
than 1/2%. As discussed previously, the evaporator was not
modeled exactly and this resulted in evaporator temperature
profile differences as depicted in Figs. 14 and 15.

Wick Pumping Tests

Two types of information were provided by the wick pumping
experiments. First, the maximum pumping capabilities of the
wick were studied to establish similarity from model to proto-
type, and second, the variation of the minimum radius of cur-
vature with liquid temperature was investigated.

In these tests the heat pipes were driven to failure by
slowly increasing the heat input by increments until the pump-
ing capacity of the wick was exceeded. Evidence that limiting
heat fluxes were associated with failure of the wicks as cap-
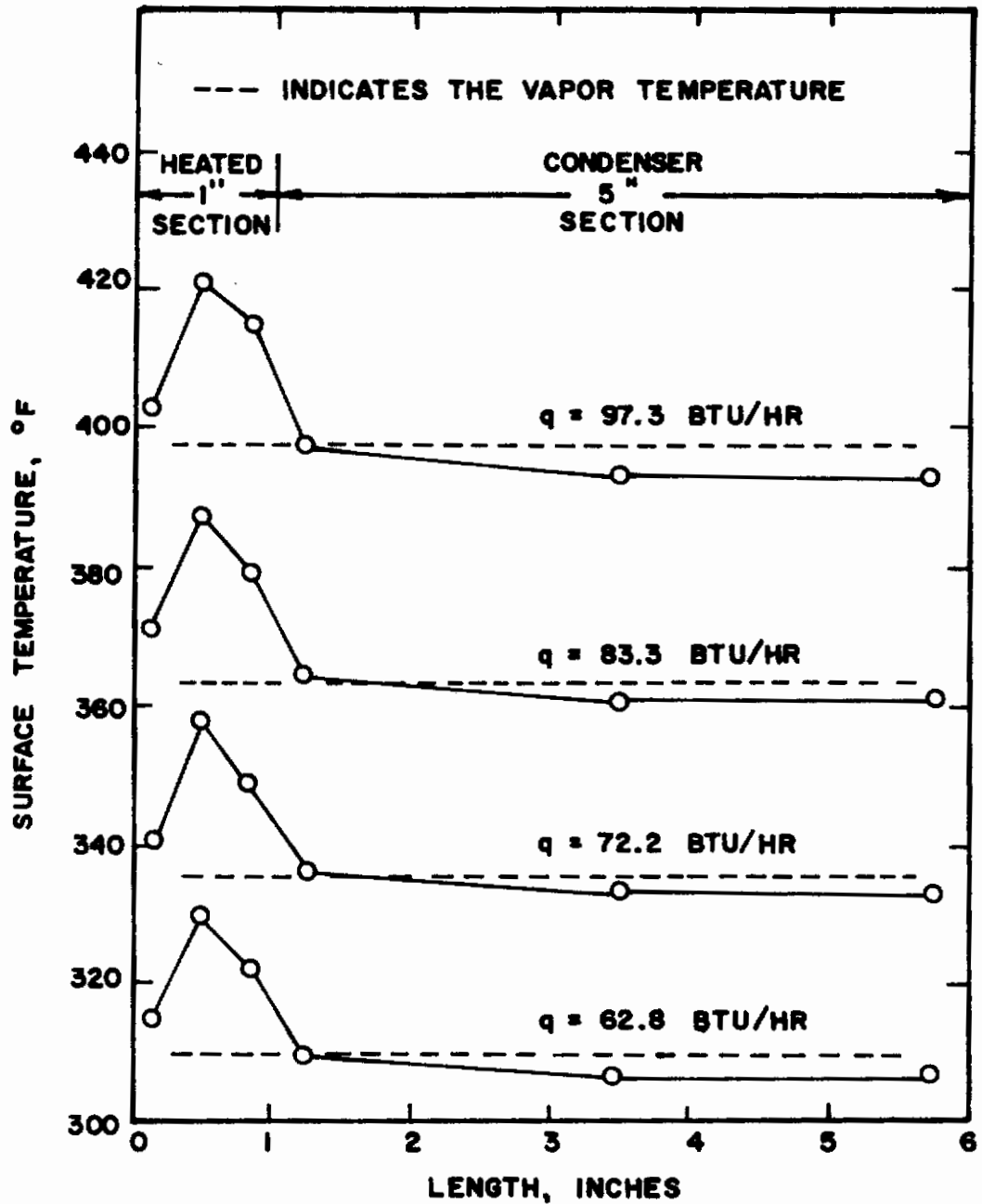illary pumps is provided in Figure 16. At the base of the

44

FIGURE 14. TYPICAL AXIAL TEMPERATURE PROFILES AS FUNCTIONS OF HEAT INPUT FOR THE MODEL HEAT PIPE
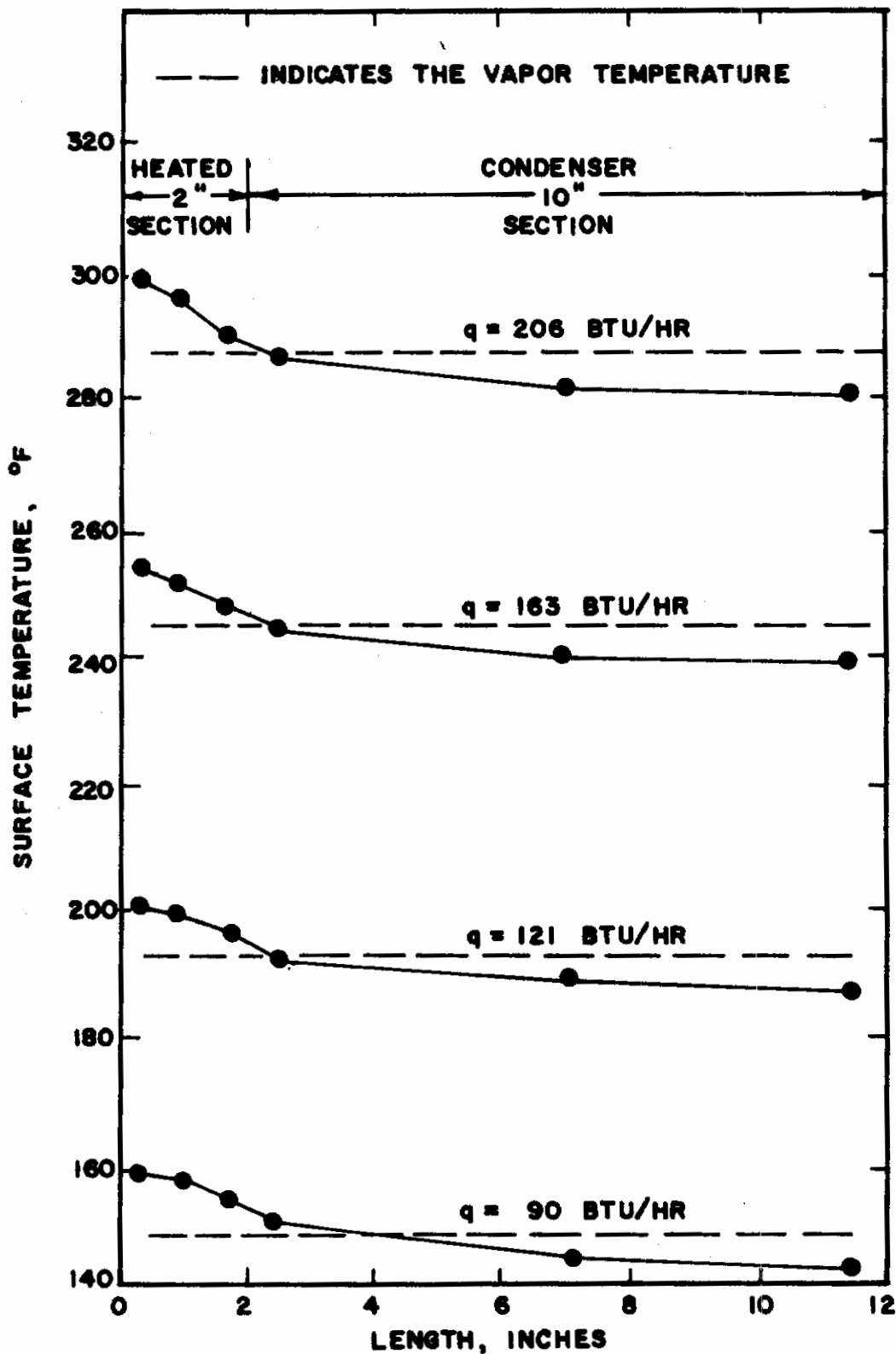
45

FIGURE 15. TYPICAL AXIAL TEMPERATURE PROFILES AS
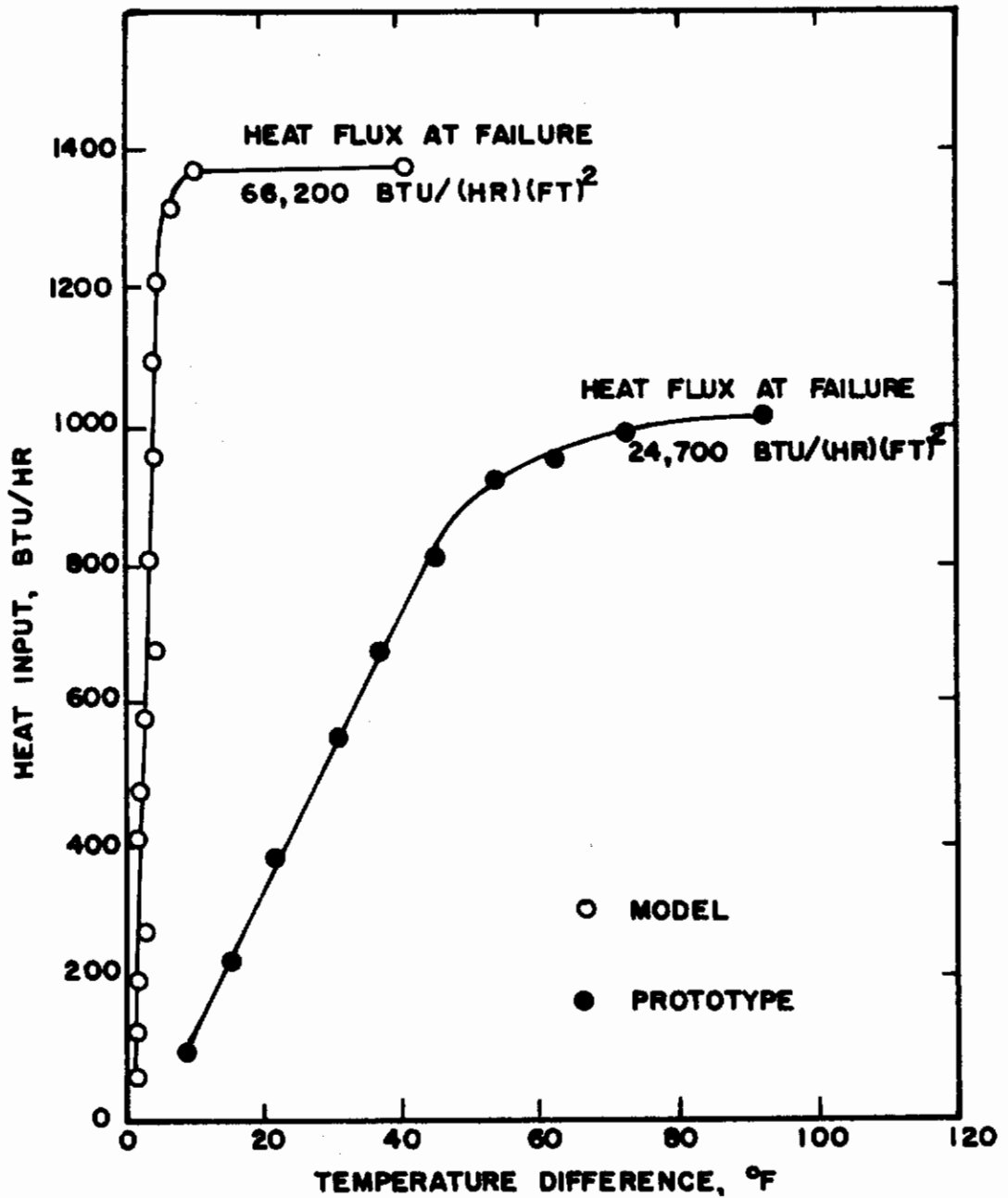FUNCTIONS OF HEAT INPUT FOR THE
PROTOTYPE HEAT PIPE

46

FIGURE 16. TEMPERATURE DROP ACROSS THE EVAPORATOR
WALL AND WICK FOR INCREASING VALUES
OF HEAT INPUT

47

heat pipe next to the heater, the temperature drop through

the wall and wick exceeded 60°F only after failure had occurred.

This low degree of wall superheat indicates that until the

pumping capacity of the wick was exceeded, liquid was present

in the wick, and vapor blockage was not impeding heat transfer.

Also, heat transfer rates never exceeded 66,200 Btu/hr-ft^2

which is lower than values normally associated with film-

boiling.

An equation for determining the maximum rate at which

heat can be transferred by a heat pipe when it is limited by

the capability of the wick to deliver adequate liquid flow

to the evaporator, has been derived from mass, energy, and

momentum considerations (3). The assumptions listed in

Section II are sufficient for this derivation. The expression

for maximum heat input is

$$q_{max} = \frac{2kA_E N}{(L_T + L_a)} \left[\frac{2}{R_{min}} - \frac{\rho_f L_T g}{\sigma_f g_c} \cos \Theta \right] , \tag{31}$$

where A_E is the area of the wick open to flow, L_T is the total

heat pipe length, L_a is the length of the adiabatic section, Θ

is the angle at which the heat pipe is elevated, and g and

g_c are the local acceleration of gravity and the gravitational

constant respectively. All values in this equation are experi-

mentally known except R_{min}.

Figure 17 shows the results of the experimental determinations
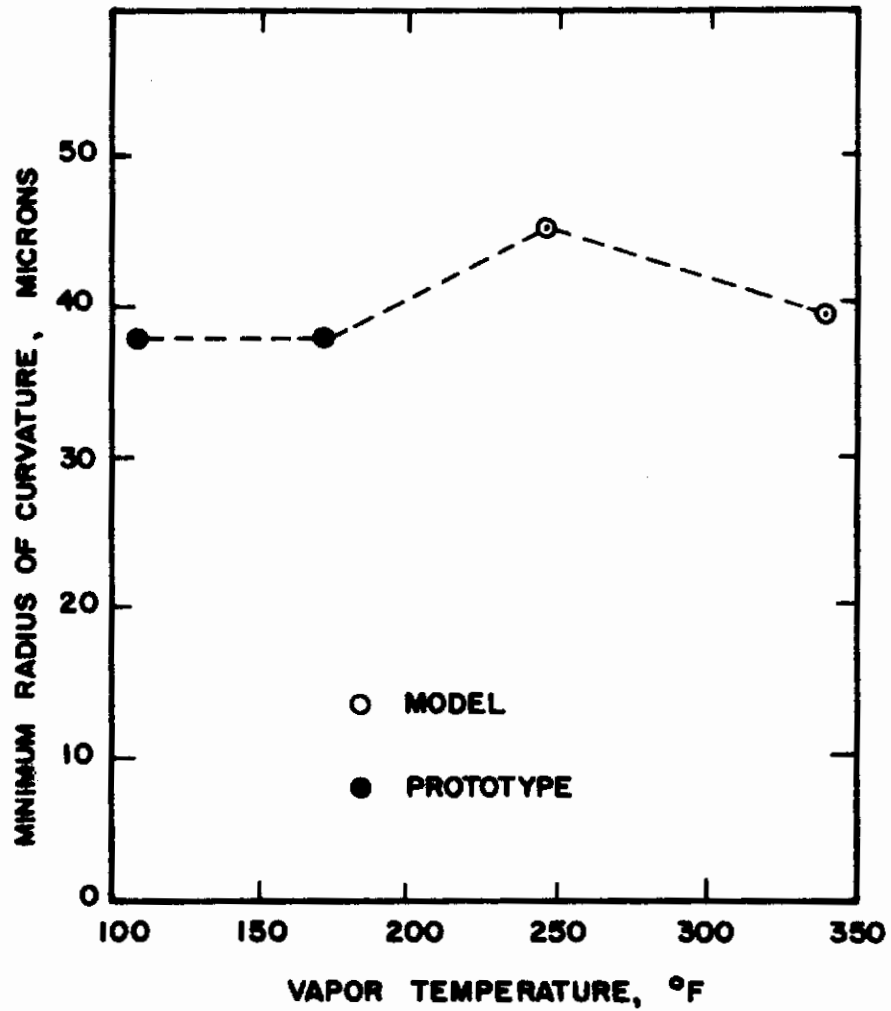
of the minimum radius of curvature. Two experimental data

48

FIGURE 17. MINIMUM RADIUS OF CURVATURE IN THE MODEL AND PROTOTYPE HEAT PIPES OVER A RANGE OF OPERATING TEMPERATURES

49

points were obtained from tests on the prototype.

Over the 250°F temperature range of experimentation, the calculated values of R_{min} varied as much as 20%. The experimental uncertainties encountered in these experiments are too large to predict R_{min} with any greater confidence. In this regard, it must be said that no predictable variation in the minimum radius of curvature was obtained over the temperature range in question.

Error Analysis for Wick Pumping Tests

The largest single source of uncertainty in the wick validation tests was k, the specific permeability of the wick. The value of k, and its bounded range of uncertainty, were determined by Kunz (5) for several kinds of materials, including the material used in these tests.

Other possible uncertainties that contributed to the total uncertainty in R_{min} are presented in Table 3. The combined uncertainties limit the determination of R_{min} to ±9.5%.

Implications of the Study

Thermal scale modeling by the technique of material preservation proved to be a very effective method for predicting prototype behavior (i.e., at a set operating point the temperature, heat flux, and mass flux are predictable) over a wide range of operating temperatures and/or heat inputs. Even

50

TABLE III

Uncertainty Bound in the Determination of R_{min}

Quantity	Source	Uncertainty
q_{max}	measured	±5.0%
k	reference 5	±9.8%
A_E	measured	±1.0%
L_T	measured	±0.5%
L_a	measured	±2.0%
N	property (measured temperature)	±5.0%
ρ_f	property (measured temperature)	±0.7%
σ_f	property (measured temperature)	±1.8%
R_{min}	calculated from above data[1]	±9.5%

[1]This uncertainty is obtained from the square root of the sum of the uncertainties squared for the parameters in Equation (31), each uncertainty weighted by the appropriate partial derivative of Equation (31).

though instrumentation loading errors were an appreciable part of the total heat input, their value could be bounded such that the quality of the results were acceptable.

The effectiveness of this modeling technique was demonstrated, in a cold wall, high vacuum environment, to a maximum heat pipe operating temperature of 400°F (the corresponding saturation pressure is over 230 psig). Tests were not performed above this temperature because of structural considerations.

Wicking tests were performed under more suitable heat transfer conditions to see if the model heat pipe was capable of predicting the maximum heat transfer capacity for the prototype heat pipe. Because of rather large experimental uncertainties in the minimum radius of curvature R_{min}, the model cannot be guaranteed to predict prototype maximum heat flux closer than ±10%. This uncertainty in the maximum predicted heat flux is directly traceable to the uncertainty in the minimum radius of curvature through consideration of Equation (22).

A second modeling technique was proposed in Section II specifying the preservation of heat flux. The most desirable feature of this modeling technique is that temperatures are approximately preserved. This favorable characteristic, however, is accompanied by several drawbacks.

Material preservation is excluded by the second technique. This means that at least one of the three materials that go into making a heat pipe must be different from model to

prototype. Most probably all three materials would have to be changed; the wick, liquid, and wall. Even by changing all three materials, there is no guarantee that the model will predict prototype behavior over a wide range of operating temperatures, since liquid properties can vary greatly with temperature.

Future circumstances might require this modeling technique which preserves heat flux and temperature; however, before the similarity relations from this report are used, they should be verified by experiment.

SECTION IV

SUMMARY OF RESULTS

The following results were obtained from an investigation of the
operating characteristics of heat pipes:

1. The similarity relations for the material preservation model-
ing technique were derived and then corroborated by experimental measure-
ments. It was observed that prototype thermal behavior could be predicted
to within 10°F over the temperature range tested (140 to 330°F).

2. A separate wicking experiment indicated that model testing could
predict prototype failure, that is failure of the capillary action in the
wick, to within $\pm 10\%$ of the total heat input to the prototype. It should
be emphasized that capillary failure was investigated in these experiments
and not failure due to boiling characteristics and/or vapor blockage.

3. It was also observed in the wicking tests that R_{min}, the radius
of curvature of the liquid-vapor interface in the evaporator under condi-
tions of maximum heat input, had no predictable variation with vapor
temperature over the span 100 to 350°F. The experimental uncertainty in
predicting the value of R_{min} is $\pm 9.5\%$ over this temperature range.

4. Since the similarity relations for the heat flux preservation
modeling technique were not verified by experiment, this method cannot be
recommended for immediate use. Furthermore, it is doubtful that this
method will ever be widely used because of the difficulties in matching
material properties from model to prototype. The one major attribute of
this modeling technique is that temperatures are preserved from model to
prototype.

REFERENCES

(1)   Vickers, J.M.F., "Thermal Scale Modeling," Astronautics and Aeronautics, May, 1965.

(2)   Miller, P.L., "Thermal Modeling in a Simulated Space Environment," Ph.D. Dissertation, Oklahoma State University, Stillwater, Oklahoma, July, 1966.

(3)   Cosgrove, J.H., "Engineering Design of a Heat Pipe," Ph.D. Dissertation, North Carolina State University, Raleigh, North Carolina, 1966.

(4)   Scheidegger, A.E., "The Physics of Flow Through Porous Media," Macmillan, 1960.

(5)   Kunz, H.R., Langston, L.S., Hilton, B.H., Wyde, S.S., and Nashick, G.H., "Vapor-Chamber Fin Studies," NASA CR-812, June, 1967.

(6)   Cotter, T.P., "Theory of Heat Pipes," Report No. LA-3246-MS, Los Alamos Laboratory, Los Alamos, New Mexico, November, 1965.

(7)   Gorring, R.L., and Churchill, S.W., "Thermal Conductivity of Heterogeneous Materials," Chemical Engineering Progress, Vol. 57, No. 7, pp. 53-59, July, 1961.

(8)   Katzoff, S., "Heat Pipes and Vapor Chambers for Thermal Control of Spacecraft," AIAA Paper 67-310, April, 1967.

(9)   Schrage, Robert W., "A Theoretical Study of Interphase Mass Transfer," Columbia University Press, New York (1953).

(10) Fowle, A.A. and F. Gabron, "Thermal Scale Modeling of Spacecraft: An Experimental Investigation" Reports on contract research by A.D. Little, Inc. for Jet Propulsion Laboratory, Pasadena, California. Phase I, Sept., 1962; Phase II, June 1963; Phase III, March 1964.

(11) Conway, E.C., and Kelley, M.J., "A Continuous Heat Pipe for Spacecraft Thermal Control," ASME Aviation and Space - Progress and Prospects, June, 1968, 655-658.

(12) Feldman, K.T., and Whiting, G.H., "Applications of the Heat Pipe," Mechanical Engineering, November, 1968, 48-53.

APPENDIX A

Differential Equations for a Heat Pipe

The differential equations describing heat pipe performance have been developed based on mass, momentum, and energy balances (3). The nine assumptions and restriction listed in Section II are sufficient for the development of these equations. Figure 18 illustrates the mechanisms of mass transfer that occur in a heat pipe.

A mass balance at any axial coordinate x requires that

$$\dot{m}_f(x) = \dot{m}_g(x) \tag{A-1}$$

Because of uniform input and output heat flux, the condensation and evaporation rates become

$$\text{at } 0 < x < L_c: \quad \frac{d\dot{m}_f}{dx} = \frac{\rho_g v_s A_c}{L_c} = C_1 \tag{A-2}$$

and

$$\text{at } -L_e < x < 0: \quad \frac{d\dot{m}_g}{dx} = \frac{\rho_g v_i A_e}{L_e} = C_2 \tag{A-3}$$

where C_1 and C_2 are constants, v_s and v_i represent suction and injection velocities, respectively, for vapor leaving and entering the vapor flow stream.

From the conservation of energy there results

$$h_f \frac{d\dot{m}_f}{dx} + q/L_c = \dot{m}_g h_g/L_c \; , \tag{A-4}$$

$$q = \varepsilon \sigma_o A_c T_o^4 \; , \tag{A-5}$$

56

EVAPORATOR | x = 0 | CONDENSER

L_e | L_c

CAPILLARY FLOW

VAPOR FLOW

r

x

EQUIVALENT VAPOR SUCTION VELOCITY, V_s

VAPOR VELOCITY PROFILE

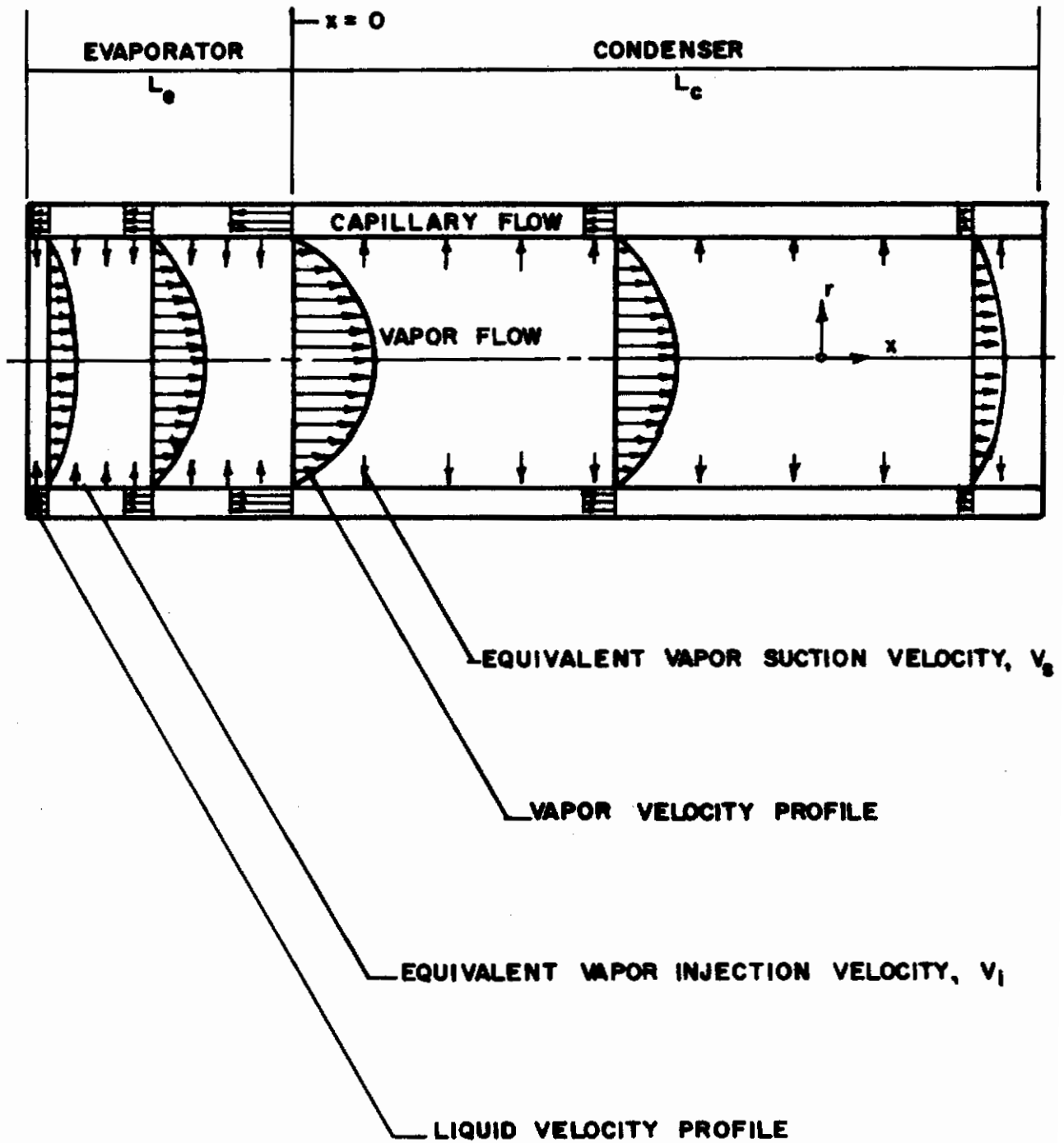EQUIVALENT VAPOR INJECTION VELOCITY, V_I

LIQUID VELOCITY PROFILE

FIGURE 18. MASS TRANSFER IN A HEAT PIPE

57

and

$$q = \frac{2\pi L_c (T_v - T_o)}{\dfrac{\ln(r_2/r_1)}{K_1} + \dfrac{\ln(r_3/r_2)}{K_2}} \quad . \tag{A-6}$$

The momentum equation for liquid flow in the wick is of the form

$$2\sigma_f \frac{d}{dx}\left(\frac{1}{R}\right) - \frac{\mu_f \dot{m}_f}{k\rho_f A_T} = \frac{1}{\rho_f g_c A_T^{\ 2}} \frac{d}{dx}(\dot{m}_f^{\ 2}) \quad . \tag{A-7}$$

In a heat pipe, the pressure drop around the liquid-vapor flow circuit must be zero, that is,

$$\Delta P_1 + \Delta P_2 + \Delta P_3 + \Delta P_4 = 0 \quad , \tag{A-8}$$

where

ΔP_1 = pressure rise, liquid to vapor, in evaporator,

ΔP_2 = pressure drop in vapor, evaporator to condenser,

ΔP_3 = pressure drop, vapor to liquid, in condenser,

and

ΔP_4 = pressure drop in the wick.

The pressure rise ΔP_1 results from the capillary forces in the wick and can be written as

$$\Delta P_1 = \frac{2\sigma_f}{R} \quad . \tag{A-9}$$

The pressure drop in the vapor ΔP_2 is obtained by solving the Navier-Stokes equations for porous pipe flow with uniform

58

suction and injection. These equations are

$$u \frac{\partial u}{\partial x} + v \frac{\partial u}{\partial r} = - \frac{1}{\rho_g} \frac{\partial P}{\partial x} + \nu_g [\frac{\partial^2 u}{\partial r^2} + \frac{1}{r} \frac{\partial u}{\partial r} + \frac{\partial^2 u}{\partial x^2}] , \qquad \text{(A-10)}$$

$$u \frac{\partial v}{\partial x} + v \frac{\partial v}{\partial r} = - \frac{1}{\rho_g} \frac{\partial P}{\partial r} + \nu_g [\frac{\partial^2 v}{\partial x^2} + \frac{\partial^2 v}{\partial r^2} + \frac{1}{r} \frac{\partial v}{\partial r} - \frac{v}{r^2}] , \qquad \text{(A-11)}$$

and

$$\frac{\partial(ru)}{\partial x} + \frac{\partial(rv)}{\partial r} = 0 , \qquad \text{(A-12)}$$

where u and v are velocities in the x and r directions, respectively, and ν_g is the kinematic viscosity of the vapor. The boundary conditions for these equations are

at r = 0: $\qquad v = \frac{\partial u}{\partial r} = 0$,

at r = r_1 and $-L_e < x < 0$: $\qquad u = 0, v = -v_i$,

at r = r_1 and $0 < x < L_c$: $\qquad u = 0, v = v_s$,

at x = $-L_e$: $\qquad u = v = 0$,

and

at x = L_c: $\qquad u = v = 0$.

The pressure drop in a condensing vapor has been derived using kinetic theory (9). The resulting equation is

$$\Delta P_3 = \frac{(2\pi R_v T_v)^{1/2}}{\alpha} \frac{d\dot{m}_g}{dx} , \qquad \text{(A-13)}$$

where R_v is the gas constant, T_v is the vapor temperature, and

α is the mass transfer accommodation coefficient.

The pressure drop in the wick ΔP_4 is obtained by solving Darcy's equation,

$$\frac{dP}{dx} = \frac{\mu_f \dot{m}_f}{k \rho_f A_T} \, . \tag{A-14}$$

Equations (A-1) through (A-14) describe the thermal behavior of a heat pipe.

APPENDIX B

Dimensional Distortion

Because of fabricational difficulties the ratio of the wick thickness dimension, model to prototype, was measured and found to be

$$(r_2 - r_1)^* = 0.480 \ , \tag{B-1}$$

instead of the prescribed value

$$L^* = 0.512. \tag{B-2}$$

The modeling Equations (28), (29), and (30), presented in Section II, were altered to reflect this 6% distortion in the wick thickness dimension.

The wick thickness does not enter into the derivation of Equation (29), and consequently this equation has not been altered from its original form, Equation (21).

Equation (30) was derived by combining Equations (6) and (14). There results

$$[\frac{LR\mu_f q}{\sigma_f k \rho_f h_{fg} A_T}]^* = 1 \ . \tag{B-3}$$

Simplifying this expression by the assumption that $R^* = k^* = 1$ and the definition that $N = \frac{\sigma_f \rho_f h_{fg}}{\mu_f}$, it becomes

$$\frac{q^* L^*}{N^* A_T^*} = 1 \tag{B-4}$$

which is the same as Equation (30) in Section II.

Heat transfer by conduction through the wall and wick of the heat pipe is also influenced, as shown in Equation (28), by changes in wick thickness. This effect is not easily traced through the modeling equations because of the series coupling of the wall and the wick in the heat transfer equations. An approximation was used to compensate for the distortion in wick thickness.

The wick thermal resistance to heat transfer by conduction, in the radial direction, was calculated by a method suggested by Gorring (7). For both the model and prototype, the wick thermal resistance to heat transfer was found to be at least 90% of the combined resistance offered by the wick and wall in series. For this reason, the correction for wick distortion was applied to both the wick and the wall of the heat pipe, even though the wall had no dimensional distortion.

In predicting $(T_v - T_o)^*$, the error introduced by the above approximation should be of the order 0.6% (i.e., 10% of 6%).

To derive Equation (28), the distortion in the thermal resistance to heat transfer was considered. The equation for thermal resistance can be expressed as

$$Z = \frac{r_2 - r_1}{K_1 A_1} + \frac{r_3 - r_2}{K_2 A_2} , \qquad\qquad (B-5)$$

where Z is the total thermal resistance to heat transfer by conduction in the radial direction, and A_1 and A_2 are the

mean areas of the wick and wall, respectively, taken at right angles to the distortion of heat flow.

Without distortion it can be shown that

$$[\frac{r_2 - r_1}{K_1 A_1} + \frac{r_3 - r_2}{K_2 A_2}]^* = \frac{1}{L^*} . \qquad (B-6)$$

With distortion in the dimensions of the wall and wick of the model heat pipe the equation becomes

$$z^* = \frac{[\dfrac{(r_2-r_1)A_T^*/(L^*)^2}{K_1 A_1} + \dfrac{(r_3-r_2)A_T^*/(L^*)^2}{K_2 A_2}]_m}{[\dfrac{(r_2-r_1)}{K_1 A_1} + \dfrac{(r_3-r_2)}{K_2 A_2}]_p} , \qquad (B-7)$$

where $A_T^*/(L^*)^2$ is indicative of how much distortion is present in the model wick thickness. Simplifying there results

$$z^* = A_T^*/(L^*)^3 . \qquad (B-8)$$

This is the thermal resistance term used in Equation (28).

APPENDIX C

A FLEXIBLE HEAT PIPE

The variety of cross sectional shapes employed in heat pipe construction has been limited only by the imagination of the designers. The most common shape to be used has been the hollow circular cylinder, primarily because of its construction convenience. It has been sufficient for many applications to fabricate the heat pipe with a straight axial centerline, i.e., without curves. Katzoff (8) suggested the use of a continuous curved heat pipe as a thermal control device for space vehicles, and this concept was later tested successfully (11). It was not until November, 1968, to the author's best knowledge, which was after completion of the experimental program reported herein, that the first published suggestion appeared to construct a flexible heat pipe which could accommodate bends and absorb vibration (12). No experimental data were furnished to substantiate this suggestion; however, reference was made to a patent disclosure dated May 2, 1967.

Conducted entirely independently of the work of Feldman and Whiting (12), this investigation has sought to demonstrate the feasibility of constructing and operating a flexible heat pipe which would be capable of being re-shaped or bent after its assembly without disturbing the heat transfer characteristics of the device. The desired objective was accomplished with a water-filled heat pipe having a fiberglass wick. The flexible portion of the unit was an adiabatic transition section between the heat input and removal sections, and, to minimize the effects of

64

testing in a standard gravity environment, it was decided to confine bending of the heat pipe to the horizontal plane.

1. EXPERIMENTAL APPARATUS

Metal tubing was employed in the heat transfer regions and the flexible capability was gained by using a thick wall plastic tubing.

The heat pipe evaporator section was constructed from an 11" piece of $1\frac{1}{8}$" diameter copper tubing (i.d. = 1.025"). A double thickness of teflon film tape was wrapped around the copper tubing and secured with epoxy cement to provide electrical insulation between the heating coil and the evaporator itself. Next, the heating coil was formed by spiral wrapping a length of Chromel-A heating ribbon (.250" x .010") around the evaporator tubing in such a manner as to give maximum coverage by the ribbon. To secure the heating element, a generous layer of high temperature epoxy was applied over the entire assembly. Finally, a narrow strip of 3/8" bakelite with two terminal lugs attached was cemented to the evaporator to provide electrical power connections, as show in Figure 18.

For the condenser section, copper tubing ($1\frac{1}{8}$" o.d.) was cut to a length of $9\frac{1}{4}$". Around this tubing, an eight-inch length of 3" o.d. copper tubing was fabricated into a concentric tube heat exchanger. Circular brass plates were used to close the annulus between the copper tubes, and inlet and outlet tubes of 5/8" copper were attached radially as shown in Figure 19.

Several materials were considered for use as the flexible tubing which joined the evaporator and condenser sections. It was desired that Teflon[R] be used; however, the only flexible Teflon[R] tubing which was
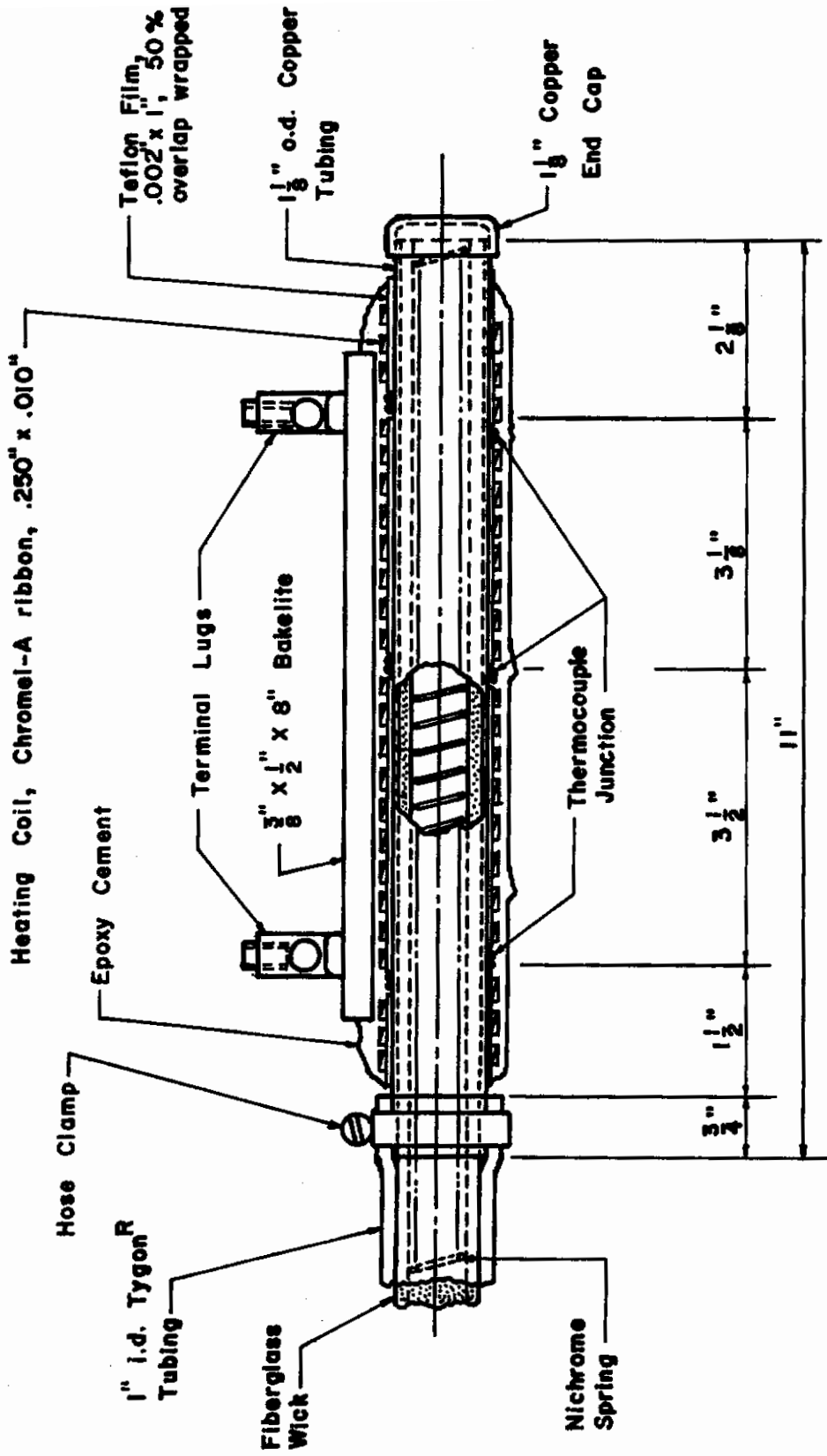
65

Teflon Film, .002" x 1", 50% overlap wrapped

$1\frac{1}{8}$" o.d. Copper Tubing

$1\frac{1}{8}$" Copper End Cap

Heating Coil, Chromel-A ribbon, .250" x .010"

Epoxy Cement

Terminal Lugs

$\frac{3}{8}$" x $\frac{1}{2}$" x 8" Bakelite

Thermocouple Junction

Hose Clamp

1" i.d. Tygon^R Tubing

Fiberglass Wick

Nichrome Spring

$\frac{3}{4}$"

$1\frac{1}{2}$"

$3\frac{1}{2}$"

$3\frac{1}{8}$"

$2\frac{1}{8}$"

11"

Figure 19. Evaporator Details.

NOTE: Silver solder all metal joints.

$\frac{1}{4}$" o.d. Copper Tubing (fill line)

Thermocouple, epoxy seal

Brass Mixing Baffles

$\frac{7}{8}$" Copper End Cap

$1\frac{1}{8}$" o.d. Copper Tubing

Hose Clamp

1" i.d. Tygon^R Tubing

Fiberglass Wick

3" o.d. Copper Tubing

Thermocouple, epoxy seal

Nichrome Spring

$\frac{5}{8}$"x3" Copper Tubing, 2 ea.
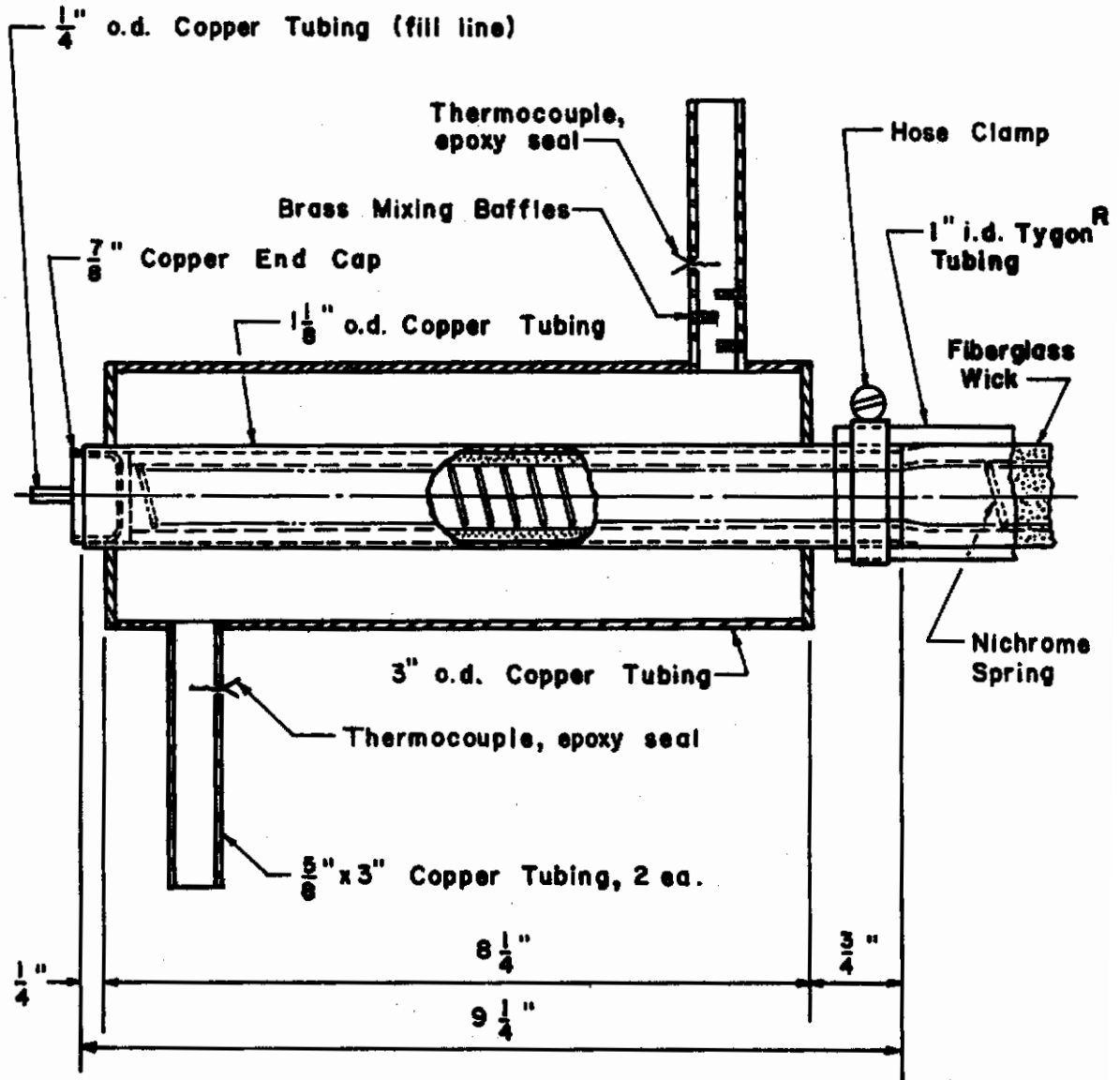
$8\frac{1}{4}$"

$\frac{3}{4}$"

$\frac{1}{4}$"

$9\frac{1}{4}$"

Figure 20. Condenser Details.

available did not have a straight, smooth inner surface, but rather an accordion type wall structure. Polyvinylchloride (PVC) tubing was also considered but tests proved that too much distortion of the circular cross section occurred during bending. Therefore, the B44-3 formulation Tygon[R] tubing was chosen as a suitable material. This plastic tubing with its excellent elastic characteristic was stretched over the ends of the evaporator and condenser sections with a 3/4" overlap and secured by hose clamps to form the outer envelope of the heat pipe.

As a wick material, woven fiberglass matting was chosen for the test apparatus. Preparation of the wick included cutting a 24" x 38" section of matting, washing it in a mild detergent solution, and thoroughly rinsing the material. After drying, the fiberglass was carefully wrapped around a 3/4" steel mandrel on which a nichrome wire spring had been previously coiled. Monofilament nylon cord was wrapped opposite the spring to temporarily secure the fiberglass which now was approximately 8 layers or 1/8" thick. The mandrel, spring, and fiberglass assembly was then inserted through the condenser until the leading end of the wick reached the outer end of the evaporator section. Next, the tension in the nichrome spring was released, allowing it to exert a uniform outward pressure on the fiberglass and thus served to insure firm contact at the container-wick interface. With the spring tension relieved, the mandrel was withdrawn. The spring and fiberglass were then trimmed to the same length as the heat pipe envelope.

To seal the heat pipe container after the wick had been inserted, external copper end caps were affixed by a soft soldering technique. The $1\frac{1}{8}$" size end cap was used on the evaporator, and on the condenser, a 7/8"

nominal external cap was expanded slightly, reversed and then soldered into place.

Figure 20 indicates schematically the assembly of auxiliary equipment which was used while testing the flexible heat pipe.

To supply power to and accurately control the resistance heater input, a variable auto-transformer was connected to a 115 volt a.c. line. The auto-transformer output was supplied to the heater through a 3 KVA step-down transformer which reduced the voltage by a 4:1 ratio.

As indicated by Figure 20, tap water was circulated through the concentric tube condenser to remove heat from the heat pipe. Included in the system to insure more accuracy and reproducibility were a water softener and a fine particle filter. A variable area flowmeter was also used to provide a visual indication of fluctuations in the coolant flow rate. Flow rate control was maintianed by means of a metering needle valve.

Instrumentation of the heat apparatus included current and voltage meters, connected as shown in Figure 20, whose readings were used to determine the electrical power input to the heating coil. The evaporator temperature was measured with six copper-constantan thermocouples which were embedded between the coils of heating ribbon at the locations shown in Figure 21. Figure 21 also indicates the positions of ten other Cu-Cn thermocouples which indicated the temperatures along or near the heat pipe. At the condenser, a thermocouple was placed in both the inlet and outlet tube flow streams to record the temperature differential of the coolant. The ambient air temperature and the barometric pressure were also recorded.
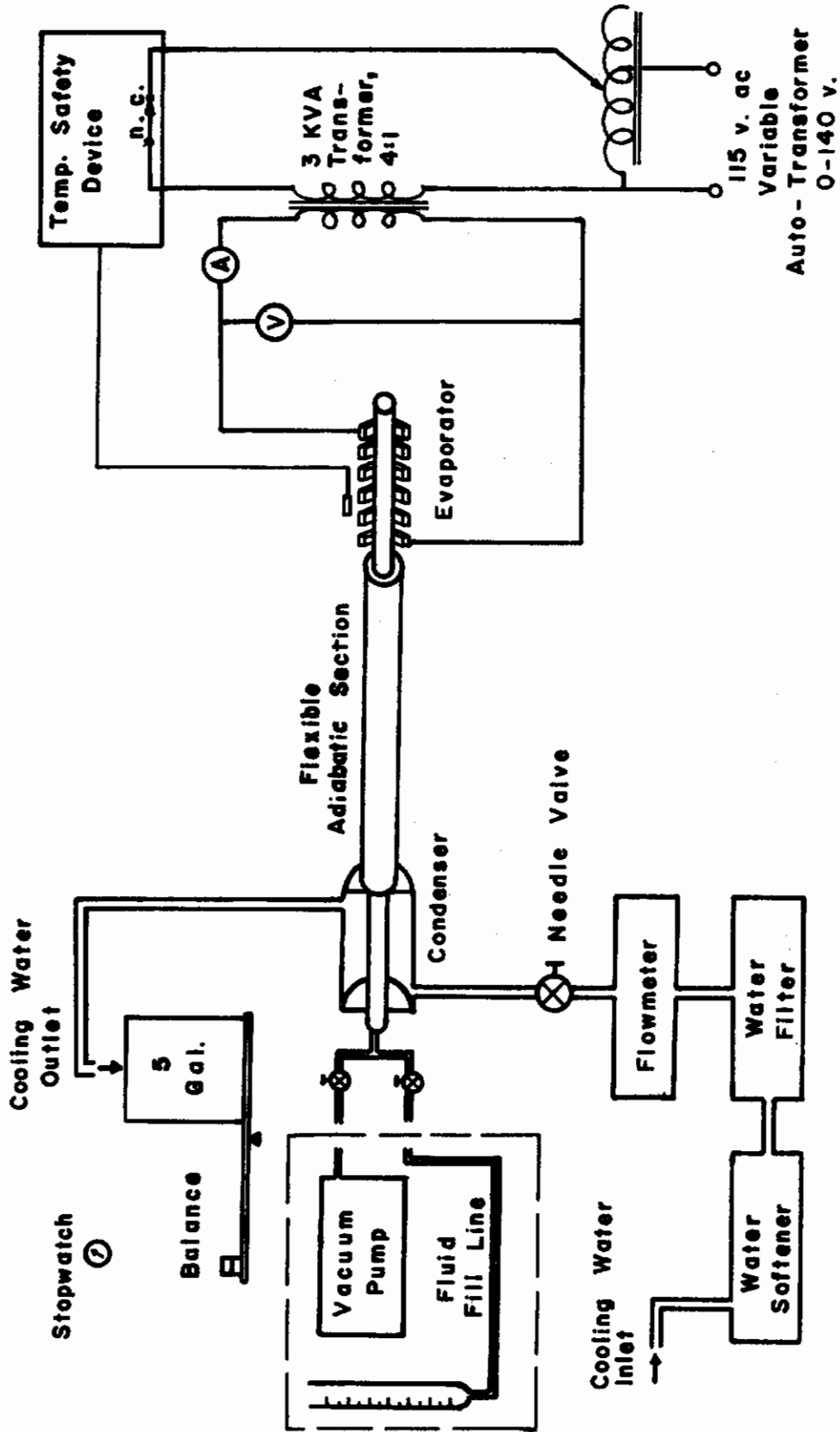
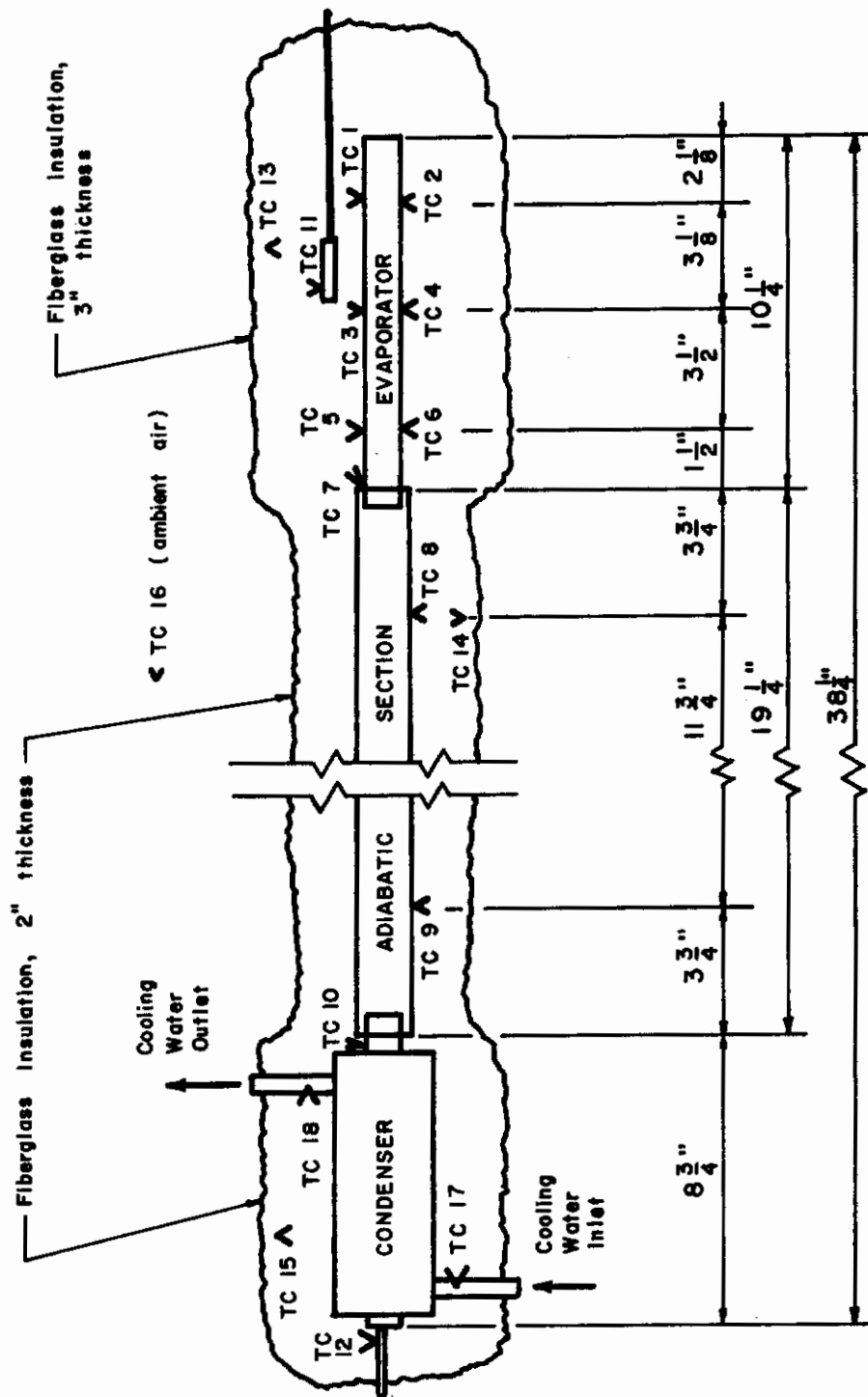Figure 21. A Schematic Diagram of the Test Assembly.

Figure 22. Thermocouple Locations.

2. EXPERIMENTAL PROCEDURE

In preparing the heat pipe for operation, it was necessary to evacuate the containment vessel and dry the wick for several hours to insure removal of entrapped air and other gasses. This outgassing procedure was accomplished by connecting the heat pipe to a high-vacuum diffusion pump with 1/4" copper tubing. A Pirani gage was used to leak test the apparatus, and no changes in the vapor pressure were noted when the joints and welds were painted with acetone. Diaphragm type vacuum valves were included to close the vacuum line and also the fill line after the heat pipe had been charged with 200 ml of distilled, deionized water. This volume of water was calculated to be the amount required to saturate the wick and provide a 20% excess. After adding the fluid and disconnecting the heat pipe from the vacuum pump, preliminary testing was initiated.

Before switching on the power supply to the resistance heater, a check of all thermocouples was made to insure that the emf output of each was the same for the room temperature heat pipe. The startup routine was then initiated. The power supply was adjusted to 9.0 amps, resulting in a voltage drop across the heating coil of 17.3 volts. Coolant flowing through the condenser was adjusted to about 4 lbs. of water per minute, and the evaporator temperature rise was observed on a millivolt-type recorder. During all tests, the startup procedure was performed with the heat pipe in the straightline configuration, i.e., position #1 in Figure 22.

Preliminary testing of the heat pipe revealed that a gradual temperature rise was experienced in the evaporator for any given heat input. This condition was attributed to a gradually increasing vapor pressure caused by the outgassing of the heat pipe material. (Application of a sealing
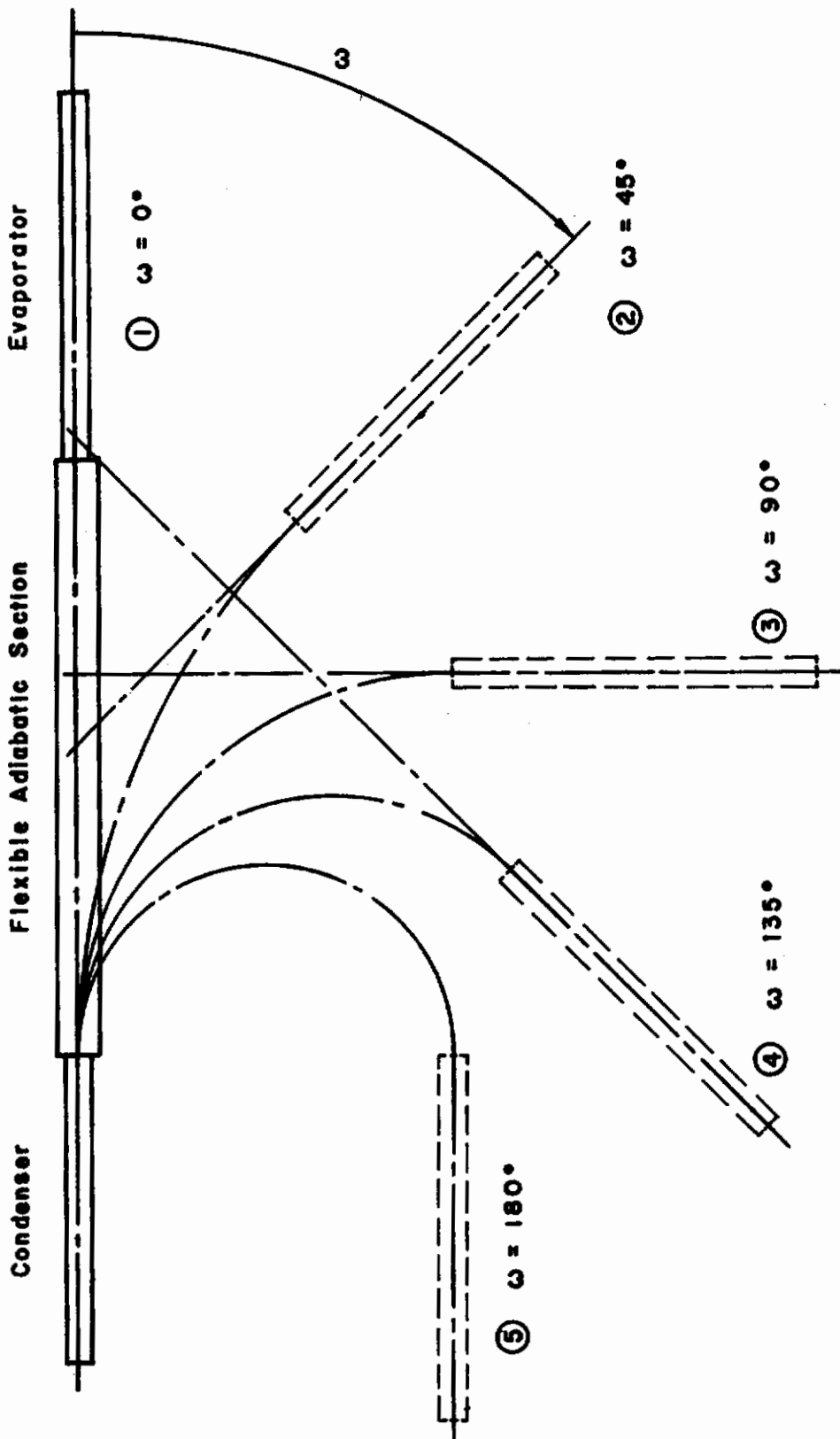
72

Figure 23. A Schematic Diagram of Test Configurations.

compound and additional testing with acetone produced no evidence of a leak in the containment vessel.) It was then decided that the objective could best be accomplished by providing an initial condition of operation which could be repeated prior to the start of each test. The condition chosen for initial reference was the level of minimum vapor pressure, and lowest evaporator temperature, inside the heat pipe with a given load. Thus, the valve on the heat pipe fill line was opened momentarily to a vacuum system to remove the non-condensable gases. During and after this removal of gases, the decreasing evaporator temperature was observed for 3-4 minutes. This gas removal technique was repeated continuously until no further reduction in the evaporator temperature was noted.

Each test of the flexible heat pipe was officially started 2.67 hrs. after the time the lowest evaporator temperature had been reached. During the course of each test, all thermocouple emf's were measured with a millivolt potentiometer. Evaporator current and voltage readings were recorded, and coolant flowrate was measured by using the stopwatch and mass balance technique. The room temperature, as well as all data mentioned above, were recorded every 30 minutes throughout each test.

At the start of each test, the heat pipe was positioned in its straight line configuration. After 0.75 hrs. had elapsed, the heat pipe curvature was changed to one of the positions shown in Figure 22. After 1.5 hrs. in the curved position, the heat pipe was returned to its original shape for approximately 1.0 hr. at which time the test was terminated.

3. RESULTS

Operation of the flexible heat pipe at a constant heat input indicated the existence of a transient temperature condition. This

74

condition was probably caused by the outgassing of the Tygon[R] tubing and the fiberglass wick which caused an internal pressure increase. A minute leak in the container is another possibility; however, previously mentioned leak detection methods failed to show a leak, and application of a sealing compound to the joints and welds failed to check the gradual temperature rise.

Because of the transient temperature, it was necessary to establish a reference for the operating heat pipe while in the 0° curvature position. With the heat input constant, 155.7 watts, the average evaporator temperature rise for two tests was found to be approximately 1.9°F/hr. In Figure 23, the average evaporator temperature change data have been plotted versus time for the two $\omega = 0°$ tests, were ω represents the angle of curvature. These data were considered to be representative of the operation of the flexible heat pipe while in the straight line configuration, and were used as a reference for the comparison of results obtained from tests of the other heat pipe positions.

Figures 24, 25, 26, and 27 indicate the results from tests of the 45°, 90°, 135°, and 180° configurations respectively. As can be seen, very favorable comparisons were obtained with the $\omega = 0°$ reference curve which is shown by a dashed line in each figure. In a few instances, the average evaporator temperature differential had a tendency to remain almost constant after a configuration change was accomplished. This has been interpreted as an indication that the capillaries in the wick material were slightly changed by bending, but that this change was subsequently removed when the heat pipe was returned to the straight line configuration.

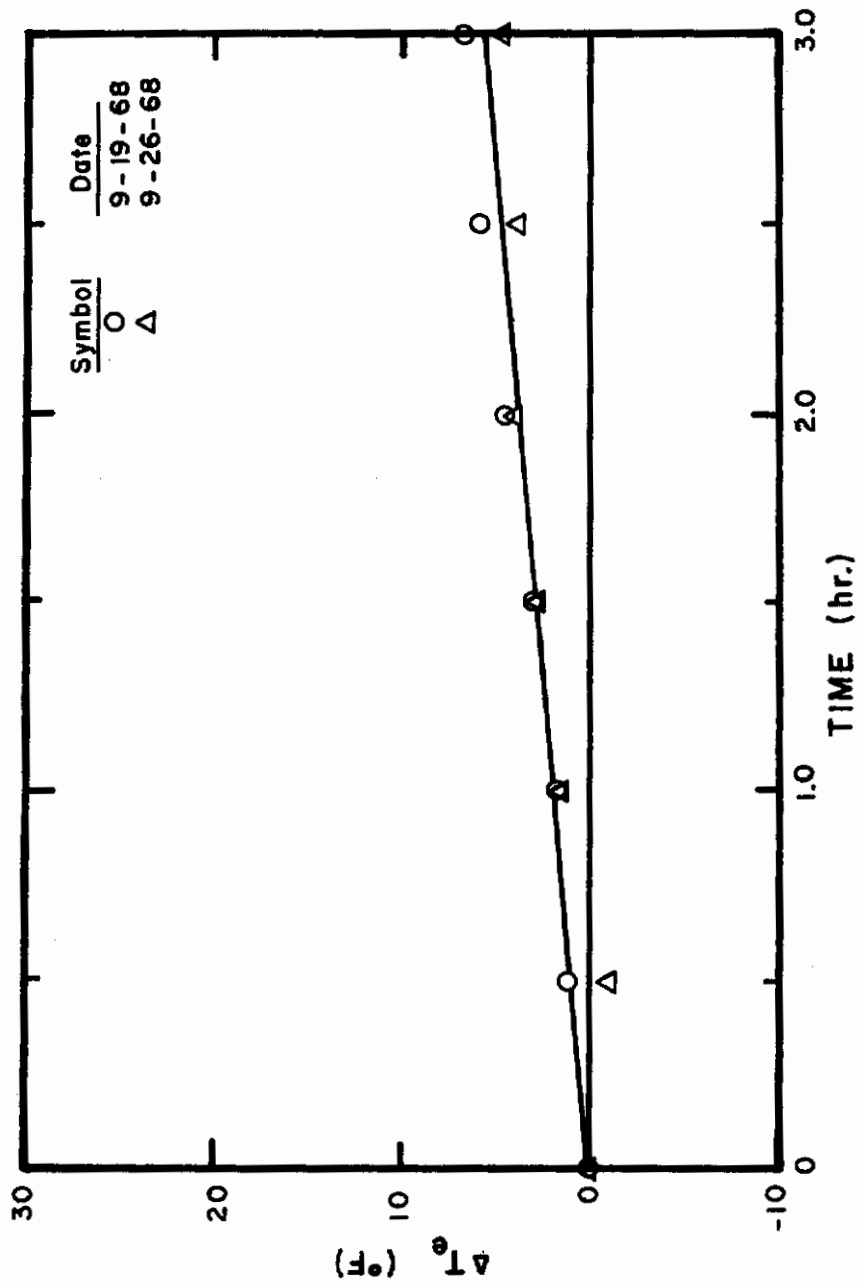Although slight differences in the average evaporator temperature

75

Figure 24. Average Evaporator Temperature Differential versus Time for O° Curvature.
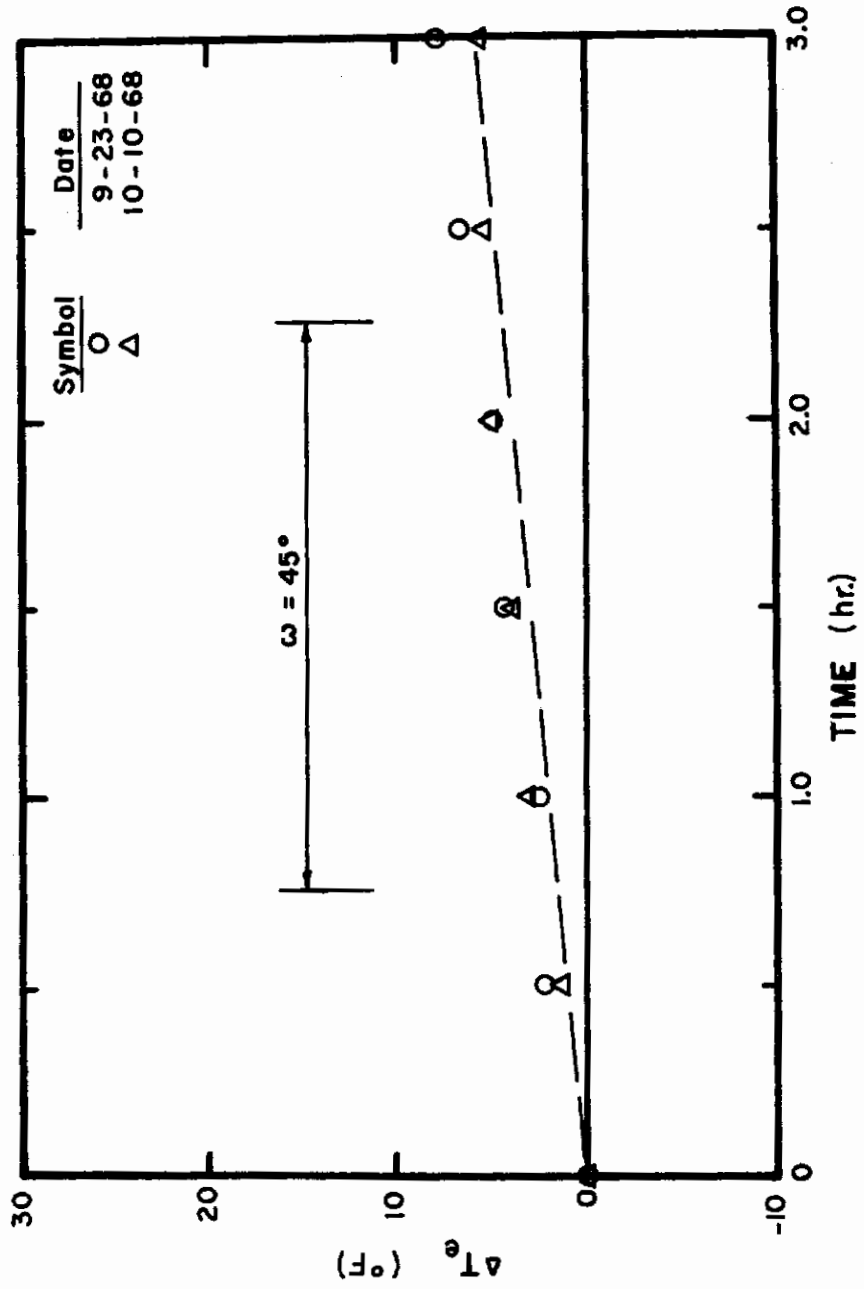
Figure 25. Average Evaporator Temperature Differential versus
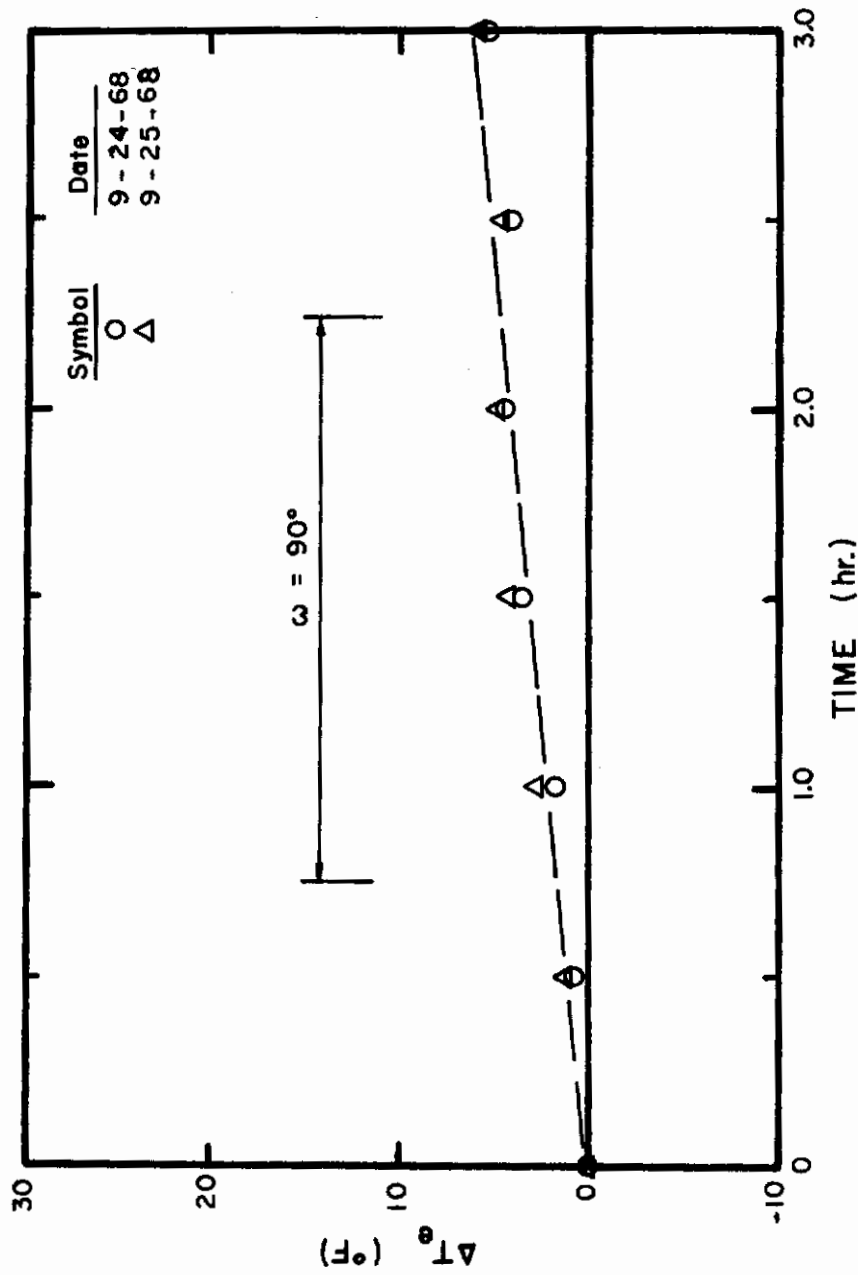Time for 45° Curvature.

Figure 26. Average Evaporator Temperature Differential versus Time for 90° Curvature.
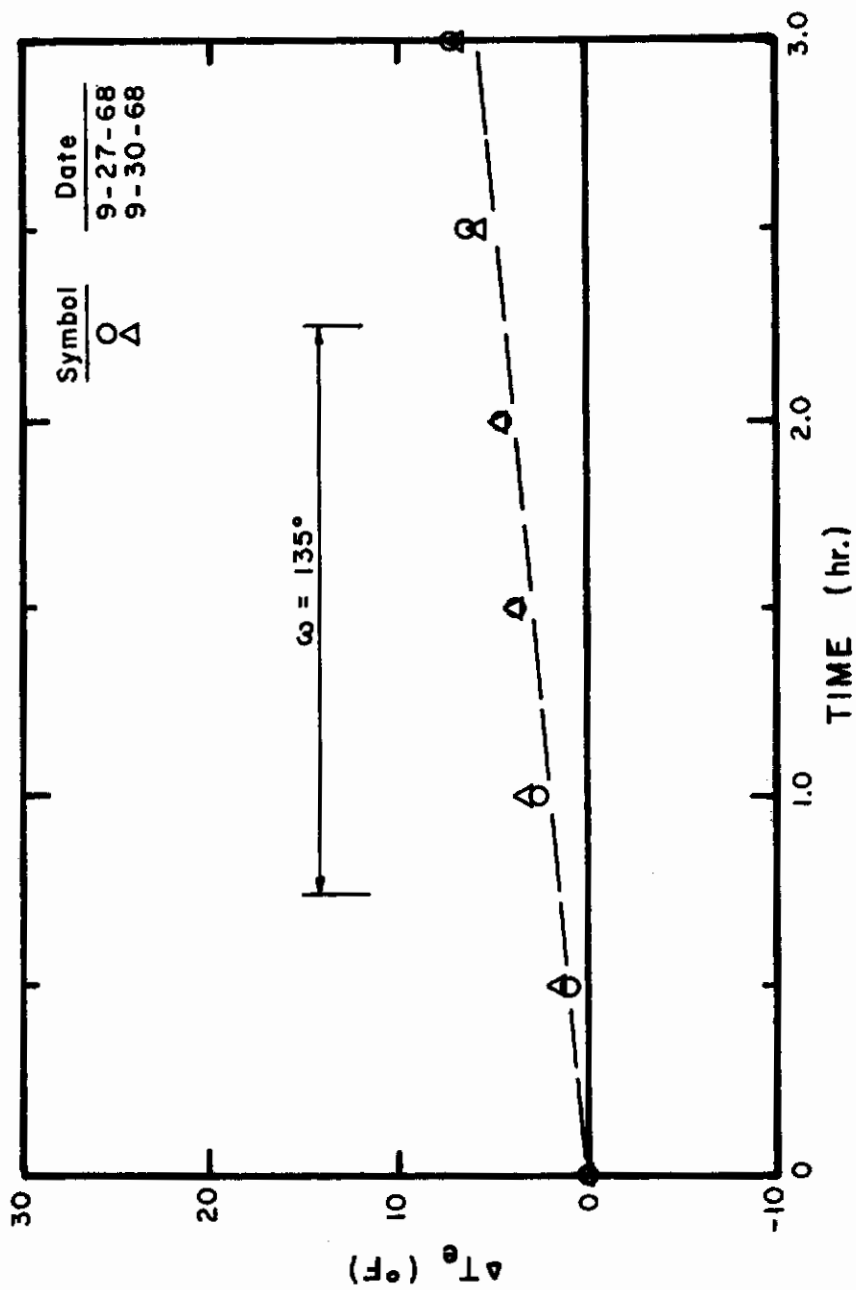
Figure 27. Average Evaporator Temperature Differential versus Time for 135° Curvature.
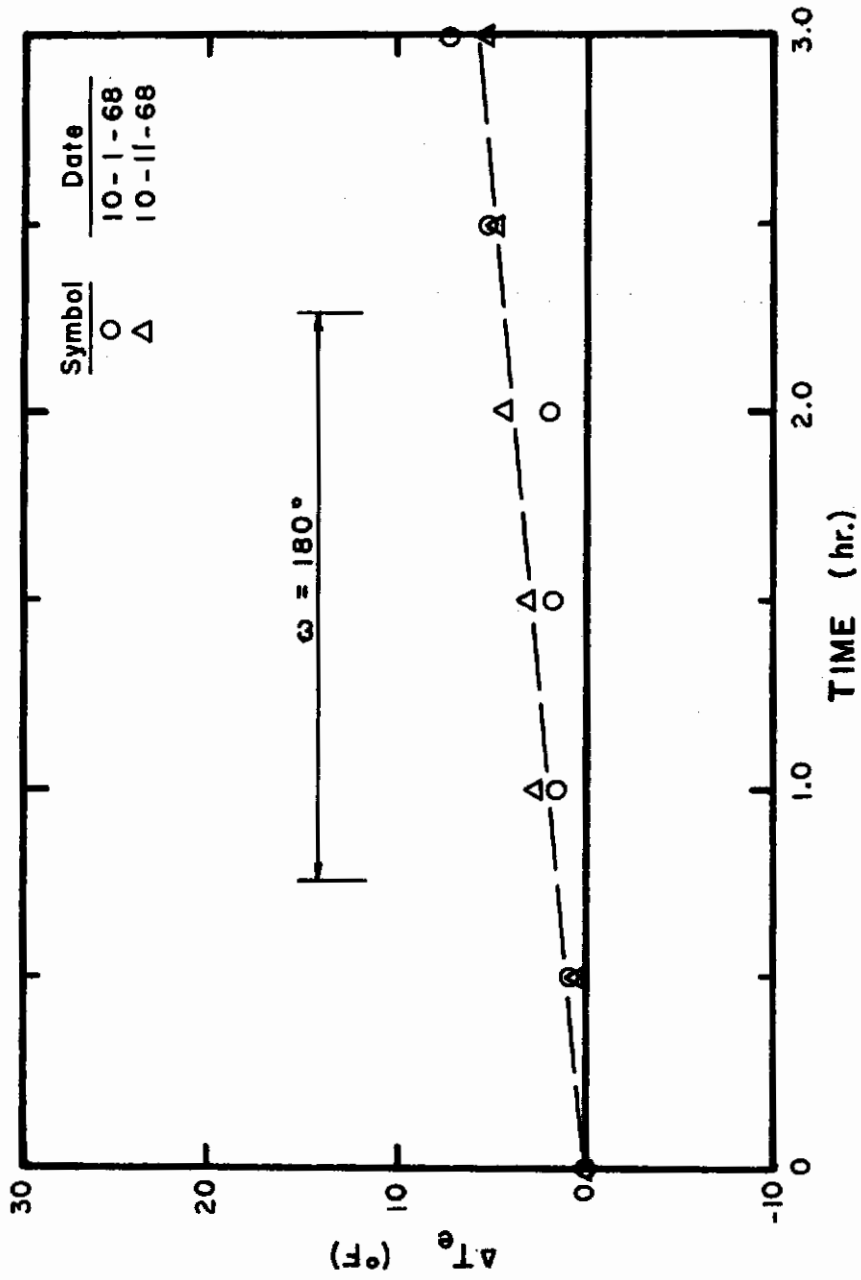
Figure 28. Average Evaporator Temperature Differential versus Time for 180° Curvature.

increase were obtained, the maximum deviation from the 0° reference curve was less than 2°F. Likewise, in the establishment of the 0° reference, the maximum difference of a particular point from the curve was also about 2 F. In general, it was determined that continued testing of the straight line configuration would produce results which displayed at least as much deviation from the reference curve as that which was found during the curved configuration tests. It is therefore reasonable to conclude that bending the flexible heat pipe in a horizontal plane does not have a significant effect on the ability to function as an efficient heat transfer device.

Several other characteristics of this flexible heat pipe also deserve mention. These traits include the evaporator temperature changes which were experienced due to changes in the input power, the maximum amount of heat which could be transported by the device, and the conditions which caused thermal runaway.

Two tests were made to establish the evaporator temperatures for various levels of heat input. Preliminary preparations for each test were the same as previously mentioned and each test was conducted over the same time frame.

For the first test, the power to the resistance heater was reduced from 155.7 watts to 70.2 watts approximately 20 minutes prior to t=0 hr. At t=0 hr., data were recorded and the power input was increased to 94.5 watts. Data were taken subsequently at half hour intervals, and upon completion of the readings for each interval, the current to the heater was incremented by 1.0 amps to a maximum value of 12.0 amps. Results are shown by the solid line in Figure 28.
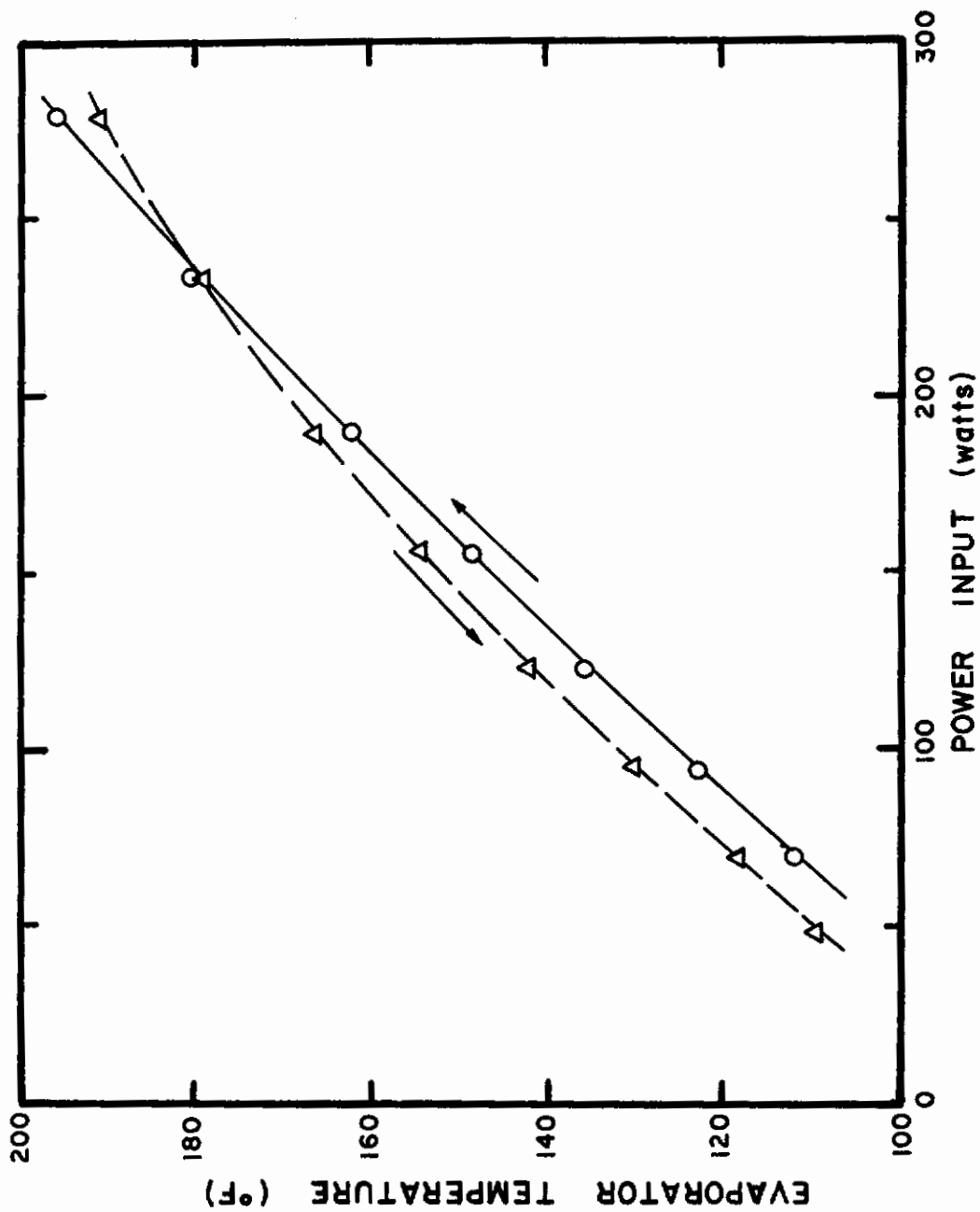
81

Figure 29. Evaporator Temperature versus Power Input.

The second trial was conducted in the same manner as the first except that the power input to the heater was varied in decreasing increments from the maximum value to the minimum. As the dashed line in Figure 28 indicates, the results obtained were slightly different from the first trial. This can be accounted by the fact that the outgassing rates of the heat pipe materials varied with the temperature and pressure inside the heat pipe. It is estimated that an average value of the two curves in Figure 28 would be the most accurate indication of the heat pipe's actual performance characteristic.

The maximum heat transfer capability of the test apparatus was not tested, as such, but it was evident that sustained operation at power levels above 280 watts could be detrimental to the device. Evaporator temperatures in excess of 190°F were obtained, and it was felt that further temperature increases would only serve to advance the risk of rupture in the flexible tubing.

Thermal runaway in the heat pipe did not occur during the comparative tests which were described above. During the preliminary tests, however, it was noted that changes in curvature when operating the heat pipe at temperatures in the 170-190°F range would sometimes cause an excessive temporary temperature increase at specific points, usually TC 1 and TC 5. In most instances, the wick was able to recover and supply sufficient working fluid to the evaporator before thermal runaway occurred. Several times, however, the amount of fluid pumped into the evaporator was so limited that almost all of the input thermal energy had to be absorbed by the wick and the copper tubing. This necessarily caused a very rapid increase in the evaporator temperature, or thermal runaway.

It was also noted during the preliminary experimentation that thermal runaway was more likely to occur when the heat input to the device was increased in large steps. For example, changing the power input to the heater from 156 watts to 278 watts would probably cause a runaway condition; increasing the power by smaller increments at regular intervals, as described previously, did not cause the heat pipe temperature control to be lost.

The validity of the results presented above was necessarily dependent upon the number and magnitude of the errors which were encountered. Detailed analysis has shown the possible sources of error to be, primarily, fluctuations in the input power to the resistance heater, heat losses through the insulation and heater cables, and the varying effects of bending upon the wick structure.

Although the amount of power input was closely attended, fluctuations in line voltage supplied to the experimental area did occur. When these fluctuations were noted, the auto-transformer was adjusted accordingly. The variance in the current supplied to the resistance heater was estimated to be ± 0.2 amps, thus making the maximum difference in power input approximately $\pm 2\%$. It should be pointed out, however, that these fluctuations, when they occurred, were always of short duration (less than 10 minutes), and the deviation from the total power input for each test was probably much less than the $\pm 2\%$ instantaneous difference.

Heat losses from the assembly were estimated for conduction of heat through the insulating material, along the thermocouple wires and through the heater power cables. Losses through the insulation around the evaporator and the flexible section were estimated to be 6 BTU/hr. and

8 BTU/hr. respectively. At the condenser, the gain of heat from the ambient air was estimated to be approximately 2 BTU/hr. Thus, the net loss of heat through the insulation was about 12 BTU/hr., or 2% of the heat input. Conduction of heat along the thermocouple wires was considered negligible; however, it was estimated that 2 BTU/hr. was conducted away by the heater cables.

Inside the heat pipe, a situation probably developed in the wick to cause a slight difference between the recorded temperatures and the actual temperature of the circulating fluid. Repeated bending and unbending of the heat pipe probably caused the wick to pull away from the wall in the evaporator and condenser sections. This condition would increase the resistance to the transfer of heat in both sections and would be character- ized in the evaporator by areas of slightly elevated temperature. Examination of the data revealed the probable existence of such a situation at thermocouples 1 and 5 during several of the tests.

DOCUMENT CONTROL DATA - R & D

(Security classification of title, body of abstract and indexing annotation must be entered when the overall report is classified)

1. ORIGINATING ACTIVITY *(Corporate author)*	2a. REPORT SECURITY CLASSIFICATION
Mechanical Engineering Department Kansas State University Manhattan, Kansas 66502	None
	2b. GROUP

3. REPORT TITLE

Investigation of Constraints in Thermal Similitude, Volume II

4. DESCRIPTIVE NOTES *(Type of report and inclusive dates)*

Final Report

5. AUTHOR(S) *(First name, middle initial, last name)*

Paul L. Miller
Francis, W. Holm

6. REPORT DATE	7a. TOTAL NO. OF PAGES	7b. NO. OF REFS
September 1969 Nov December 1969	85	12

8a. CONTRACT OR GRANT NO.	9a. ORIGINATOR'S REPORT NUMBER(S)
F33615-68-C-1017	
b. PROJECT NO.	None
c.	9b. OTHER REPORT NO(S) *(Any other numbers that may be assigned this report)*
d.	AFFDL-TR-69-91 Volume II

10. DISTRIBUTION STATEMENT

This document has bee approved for public release and sale; its distribution is unlimited.

11. SUPPLEMENTARY NOTES	12. SPONSORING MILITARY ACTIVITY
	Environmental Control Branch Vehicle Equipment Division AF Flight Dynamics Laboratory Wright-Patterson Air Force Base, Ohio 45433

13. ABSTRACT

The studies described in this report clarify the effects of some of the limitations imposed by the laws of thermal similitude, and determine the thermal modeling laws for a heat pipe.

In Volume I solutions were presented for the steady-state temperature distribution and heat transfer in a radiating fin having temperature dependent thermal conductivity. Using these solutions, modeling prediction errors were determined for fin type prototype/model systems with dimensional distortions, with material having temperature dependent thermal conductivity, and with low prototype temperatures. These prediction discrepancies ranged from very small errors to errors in heat transfer rate as high as 75% in a severely distorted model.

In Volume II the thermal modeling laws for a heat pipe were derived and experimentally verified. It was observed that prototype thermal behavior could be predicted, from model data, to within 10 F over the temperature range tested (140 to 330 F). Heat pipe failure due to capillary failure was also predictible to within $\pm10\%$.

A flexible heat pipe was also designed and experimentally tested. Performance was not degraded under conditions of bending.

DD FORM 1473
1 NOV 65

14. KEY WORDS	LINK A		LINK B		LINK C	
	ROLE	WT	ROLE	WT	ROLE	WT
thermal modeling						
heat pipe						
thermal radiation						
radiating fins						
variable conductivity fin						
fin temperature distribution						
thermal similitude						